Review of the recent advances and applications of LIBS-based imaging

L. Jolivet, M. Leprince, S. Moncayo, L. Sorbier, C.-P. Lienemann, Vincent Motto-Ros

▶ **To cite this version:**

L. Jolivet, M. Leprince, S. Moncayo, L. Sorbier, C.-P. Lienemann, et al.. Review of the recent advances and applications of LIBS-based imaging. Spectrochimica Acta Part B: Atomic Spectroscopy, 2019, 151, pp.41-53. 10.1016/j.sab.2018.11.008 . hal-01983630

HAL Id: hal-01983630
https://ifp.hal.science/hal-01983630v1

Submitted on 16 Jan 2019

HAL is a multi-disciplinary open access archive for the deposit and dissemination of scientific research documents, whether they are published or not. The documents may come from teaching and research institutions in France or abroad, or from public or private research centers.

L'archive ouverte pluridisciplinaire **HAL**, est destinée au dépôt et à la diffusion de documents scientifiques de niveau recherche, publiés ou non, émanant des établissements d'enseignement et de recherche français ou étrangers, des laboratoires publics ou privés.

Review of the recent advances and applications of LIBS-based imaging

L. Jolivet[1,2], M. Leprince[1], S. Moncayo[1], L. Sorbier[2], C-P. Lienemann[2], V. Motto-Ros[1*]

[1] *Institut Lumière Matière UMR 5306, Université Lyon 1 - CNRS, Université de Lyon 69622 Villeurbanne, France*

[2] *IFP Energies nouvelles, Rond-point de l'échangeur de Solaize, BP 3, 69360 Solaize, France*

[*]Corresponding author: Dr. Vincent Motto-Ros (vincent.motto-ros@univ-lyon1.fr)

Keywords: LIBS, elemental imaging, laser scanning, mapping

Abstract

During recent years, important developments have been achieved in the application of laser induced breakdown spectroscopy (LIBS) for elemental imaging. The aim of this review is to report recent instrumental configurations, data processing methodologies and applications related to LIBS-based imaging. In the first section, different instrumental alternatives of LIBS for qualitative or quantitative imaging measurements are presented, including the scanning configuration, focusing systems, laser properties, and spectral detection tools. The second section reviews the different LIBS imaging data processing methodologies that have been proposed. Finally, the last section of this review reports the wide variety of laboratory applications that have benefited from LIBS mapping techniques, such as those in the biomedical, geological and industrial fields.

1. Introduction

In laser induced breakdown spectroscopy (LIBS), a single laser shot occurs at the sample surface, producing a plasma whose light emissions are collected and analyzed using an optical spectrometer [1–5]. Since this technique was first used for spectrochemical analysis of surfaces in 1962 [6,7], the LIBS technique and its applications have advanced tremendously. Several technological and analytical milestones of this technique such as the introduction of double-pulse LIBS [8], commercialization of handheld systems [9], development of molecular isotopic analysis (LAMIS) [10,11], single particle analysis [12], nanoparticle enhanced LIBS (NELIBS) [13–15], and calibration free procedures [16], use of chemometrics [17–19], coupling with other techniques and exploration of Mars by the NASA Curiosity Chemcam [20,21] have made LIBS a highly versatile and adaptable technique.

Recent years have seen a growing trend towards analytical techniques capable of conducting spatially resolved analyses of surfaces for industrial, nanotechnology, geological and biomedical applications. Depending on the application, spatially resolved measurements are required to provide a better understanding of the sample surface composition with significant advantages over conventional bulk analyses. The recent developments of the LIBS technique and its simplicity of use have allowed the development of systems capable of performing multielement imaging analyses of major and trace elements with ~ 10 μm (or lower) spatial resolution at fast acquisition speeds up to kHz per pixel [22–25]. Both conventional LIBS and LIBS-based imaging share the same principles of measurement; however, in the latter, the laser-induced plasma is generated at different positions on the sample surface in a predefined sequence covering the region of interest. After extracting the line intensities associated with the elements of interest from each recorded spectrum, the elemental maps are then built to obtain the corresponding elemental images. Spatially resolved LIBS has attracted increasing attention and is currently established as a new LIBS development axis. Indeed, LIBS-based imaging provides unique features and complements gold standard elemental imaging methods such as laser ablation inductively coupled plasma mass spectrometry (LA-ICP-MS), secondary ion mass spectrometry (SIMS), synchrotron and laboratory X-ray fluorescence (μXRF) [26,27], and electron probe microanalysis (EPMA) [28–31].

In recent years, the LIBS community has shown an increased interest in LIBS-based imaging applications, as reflected by the exponential growth of publications, with more than 20 works published during the last year. To the best of our knowledge, the first works reporting spatially resolved LIBS analyses dated from the 1990s [32–37]. In the 2000s, the reference works of D. Menut *et al.* [23], H. Bette *et al.* [24] and J. Laserna *et al.* [37–42] established the basis of space-resolved LIBS and paved the way for the development of a large number of applications. These works

demonstrated the possibility of reaching µm-scale resolution by focusing a UV laser pulse of several micro joules with an objective microscope for the quantitative analysis of cerium in ceramics with a limit of detection (LOD) of 1 wt % [23], to perform multielemental LIBS scanning at a kHz acquisition rate with the aim of investigating inclusions in steel [24], and the possibility of scanning large sample surfaces and performing 3-dimensional analyses [41]. In the early 2010s, the release of new faster and more sensitive detectors to the market boosted the development of LIBS-based imaging. The latest results regarding the use of laser spectrometry in biomedical applications have again highlighted LIBS-based imaging as a valuable investigation tool that is highly versatile and easily implemented for routine elementary investigations [43,44].

In this manuscript, we aim to review the recent methodological advances and applications of LIBS-based imaging. In 2013, V. Piñon *et al.* [45] published a first review that covered the chemical mapping of materials up to the year the review was published. In this review, we focus on describing the advances in LIBS imaging instrumentation, data processing for image analysis and applications published during the last 6 years. This review is dedicated only to LIBS mapping (i.e., the ability to create a map or an image of a sample surface) for laboratory applications. Studies relating to 1-dimensional space-resolved LIBS (either as a lateral or depth profile) [46,47], geographical mapping [48–50] or in situ mapping with handheld systems [51,52] are not considered. This manuscript is organized as follows. First, we describe the instrumental configurations most often found in the literature. We then review the different methodologies of data processing and the calibration protocols reported for LIBS-imaging, and the last section describes the application fields where LIBS imaging has been applied, including the characterization of geological, industrial and biomedical materials.

2. LIBS imaging instrumentation

2.1 Instrumental configurations

As mentioned above, the principle of any LIBS imaging instrumentation is based on the generation of a series of plasmas at different positions on the sample following a scan sequence (c.f. figure 1a). Each spectrum is then processed to build the corresponding elemental maps. The step size (i.e., the distance between two consecutive laser shots) then defines the resolution of the imaging measurement. In general, the lateral resolution is limited by the surface damage around the ablation crater. Therefore, it is inadvisable to overlap consecutive laser shots, since in this case the repeatability of the measurement is degraded [53–55].

Two possible laser ablation modes have been reported in the literature: continuous measurement and pixel by pixel scanning. In the continuous laser ablation mode (c.f. figure 1b), the sample is moved in the X-direction at a translation speed synchronized with the laser frequency rate by line scan. After completing the line, the sample is translated in the Y-direction by the set lateral resolution and comes back in the X-direction, completing a new line. To acquire the correct number of spectra, this mode requires either a beam shutter working at the laser frequency rate (in which case the laser is fired continuously) [44] or a control system that delivers a predefined number of shots per line in burst mode [56–58]. For the pixel by pixel scanning mode (c.f. figure 1c), the laser delivers *k* number of laser shots at the same position; afterward, the sample is moved in X (or Y) by the step size, and the operation is repeated following the programmed sequence [55,59–67]. Compared with the pixel by pixel scan mode, continuous scanning has the advantages of a higher operating speed and better accessible resolution since less damage is done to the sample by one shot than by a series of shots; however, the analysis has to be performed in a single shot configuration (no possibility to accumulate the signal at a fixed position). Additionally, the continuous scanning mode requires specific considerations for the sample preparation since no cleaning shots can be performed prior the analysis, whereas step by step scanning mode allows for the application of cleaning shots and a 3-dimensionnal experiment to be performed [45].

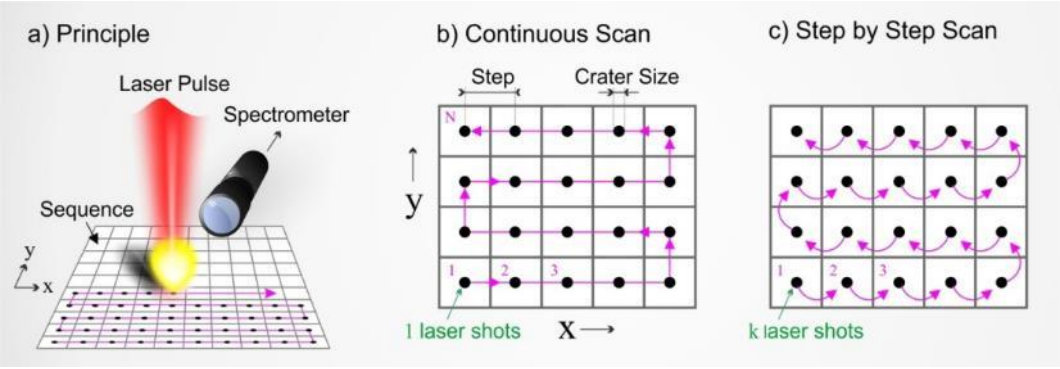

Fig. 1. Principle of LIBS scanning and principal configurations of measurement.

The vast majority of LIBS imaging instruments rely on an XY stage that moves the sample surface instead of moving the laser beam. This approach is chosen because of a greater collection efficiency from a fixed plasma plume. However, for applications such as online control that require a large sample surface to be scanned at a high frequency rate, kHz or higher, the measurements can only be performed by moving the laser beam. Recently, K. Rifai *et al.* reported the elemental imaging of 16 cm^2 of mine core samples at a kHz acquisition rate in only a few minutes by using this approach [68].

2.2 *Laser ablation and focusing*

The focusing systems and the properties of the laser source (wavelength, pulse energy, and pulse width) may be critical when building a LIBS-based imaging system. Various ranges of focusing properties and accessible resolutions can be found in the literature (c.f. figure 2a and supplementary table 1). However, two main focusing configurations are distinguished: macroscopic and microscopic. For the macroscopic configurations, the laser beam is focused by one or several lens with a focal length of several centimeters and generates ablation craters of approximately 600 µm in diameter [69–72]. For the microscopic configurations, an objective microscope (magnification higher than x5) with a focal length of several millimeters is used to focus the beam. This configuration allows the ablated material to be reduced (down to sub ng), reaching spatial resolutions of several micrometers, as demonstrated on ceramic samples [23] and on an epoxy embedded organ [73]. Moreover, in the microscopic configurations, a constant gas flow, usually Ar, can be directed to the plasma region, improving the emission signal compared with ablation in air [23,44,52,59,63,74,75]. Other gases such as He or mixtures of He-Ar have also improved the ablation efficiency. C. D. Quarles *et al.*, demonstrated that a He flow increases the fluorine LOD by several orders of magnitude [76]. S. Darwiche *et al.* investigated the effects of the composition of the mixture and showed that the maximum signal to background ratio is reached with a mixture of 85/15% He to Ar at 60 mBar [77]. B. T. Manard *et al.* reported a mixture of He and Ar at 0.9 L/min as optimal for simultaneous LA-ICP-MS and LIBS measurements [78]. Finally, M. Bonta *et al.* reported the advantages of using a He-Ar mixture with a flow rate of 0.8 L/min for each gas [79] or flow rates of 0.9 L/min of He and 0.3 L/min of Ar [80].

With respect to the laser properties, i.e., laser wavelength, pulse energy and duration, many different configurations can be found in the literature (c.f. figures 2b, 2c, and supplementary tables 2 and 3). The trend is to use laser energies of several hundreds of µJ in the microscopic mode, 0.4 mJ [81], 0.3 mJ [82], 0.2 mJ [55], 0.16 mJ [83], 0.1 mJ [78], and 0.04 mJ [63], and several tens to hundreds of mJ in the macroscopic mode, 60 mJ [69,72], 80 mJ [84], 120 mJ [85], and 150 mJ [86]. Nanosecond Nd:YAG lasers either in their fundamental wavelength [51,58,66,67,87–90] or in the second harmonic [82,91–93] are used in the vast majority of applications. Higher harmonics are used to a lesser extent [46,76,79,81,94–97]. Other laser sources such as Nd:YLF working at 1047 nm [98,99] or a KrF excimer laser at 248 nm [100] have also been proposed. In addition, several groups have developed femtosecond (fs) experiments. This type of laser guarantees better control of the ablation process but also a lower plasma emission. V. Zorba *et al.* demonstrated the possibility of reaching sub-micrometer resolution using a frequency doubled Ti:Sapphire laser delivering 100 fs pulses [101]. Other examples using Ti:Sapphire lasers operating at 800 nm [102] and at the second

harmonic [63] have been reported, as has a frequency tripled (343 nm) diode-pumped ytterbium laser [78,83].

Recently, attention has been focused on double pulse (DP) ablation to improve the signal to noise ratio with respect to the single-pulse approach. Several examples have been proposed by the group of V. Palleschi, demonstrating a signal enhancement of approximately one order of magnitude by using a collinear configuration [103,104]. J. Kaiser *et al.* have also reported significant improvements when using an orthogonal double pulse configuration compared with a single-pulse, either with a first laser pulse in the visible range (532 nm) [105,106] or in the UV range (266 nm) [54,107,108], followed by a second laser pulse in the IR range (1064 nm) to reheat the plasma. M. Abdelhamid *et al.* explored the feasibility of imaging explosive residues in human fingerprints with an experimental configuration based on optical catapulting–LIBS. A first pulse with an irradiance below the plasma formation threshold impacts one side of a glass slide, producing a shock wave that ejects the material (optical catapulting), then a second laser pulse that is perpendicular to the first analyzes the material, obtaining a LIBS spectrum [109].

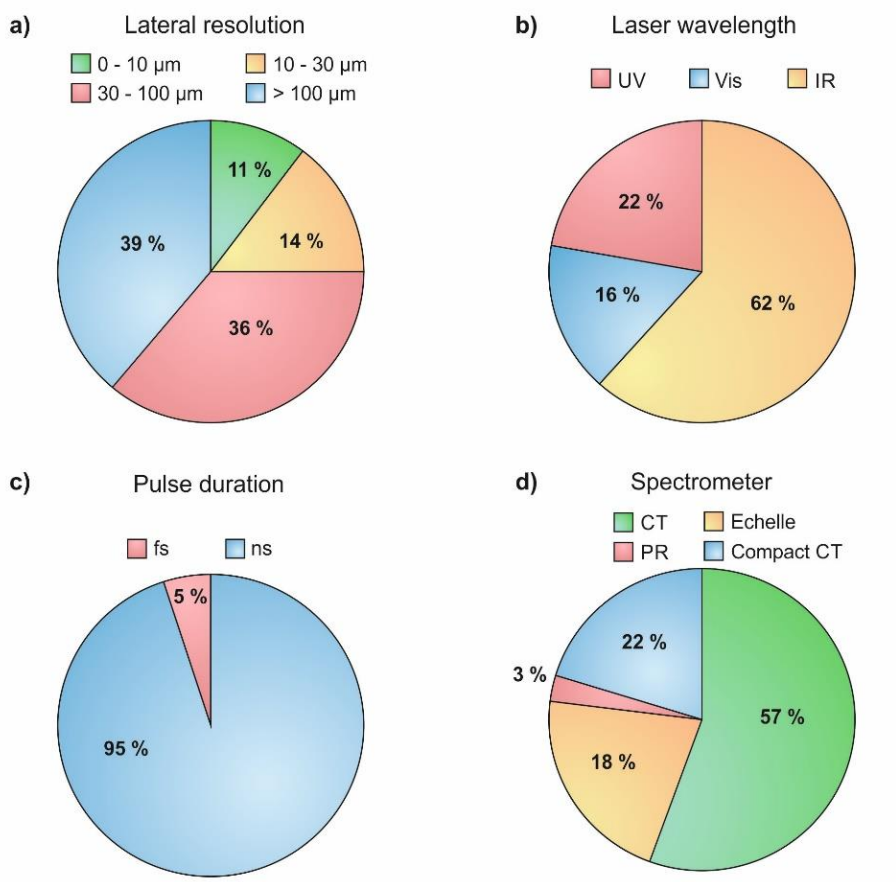

Fig. 2. Configurations used for LIBS-based imaging since 2012. a) Spatial resolution ranges. b) Laser wavelengths and c) pulse durations. d) Types of spectrometers. CT: Czerny Turner spectrometer, PR: Pashen Runge spectrometer.

2.3 Spectral detection

Another critical part of a LIBS instrument is the spectral detection system. The spectral resolution, sensitivity, operating speed and the wavelength range covered are directly related to the type of the spectrometer and detector employed and define the performance of the system. Several types of spectrometers and detectors are available on the market and the specifics of each application determine the selection. In LIBS-based imaging literature, Echelle spectrometers and Czerny-Turner (CT) spectrometers are the most widespread, although Paschen–Runge (PR) spectrometers have also been employed (c.f. figure 2d and supplementary table 4).

Focusing on their performances for use in LIBS-based imaging, each spectrometer has advantages and drawbacks. Echelle spectrometers have the great advantage of covering a broad spectral range, which is especially suitable for multielemental detection (typically extending from UV to near infrared), but these spectrometers have lower sensitivity and operating speed compared with the others. The entrance slit in an Echelle spectrometer is typically ~50 µm, which reduces the amount of light that effectively reaches the diffraction grating and limits its sensitivity. Moreover, Echelle spectrometers need to read the whole charge-coupled device (CCD) image to obtain the spectrum, which results in an increase in the readout time and reduces the acquisition rate and operational speed to only several Hz. In the literature, Echelle spectrometers have been successfully used either coupled with intensified CCD (ICCD) [60,63,83,94,99,110–115] or electron multiplying CCD (EMCCD) cameras [93].

CT spectrometers have greater sensitivity because of a larger entrance slit. Moreover, three or four different gratings are equipped within the same spectrometers, which allows for adaptation of the sensitivity and spectral range as a function of the application. The acquisition rate is also faster when used coupled with ICCD detectors, allowing for time-resolved measurements and operational speeds up to 100 Hz in full vertical binning mode (FVB) [56]. CT spectrometers also suffer from a major drawback: their limited spectral range of detection, which is typically from ~20 nm with 2400 l/mm grating to ~80 nm with 600 l/mm grating, which limits the number of elements able to be detected simultaneously [25,50,55,58,72,76–78,81,82,87,95,116–119]. Several groups have proposed using several CT spectrometers simultaneously during measurement [56,57,85]; however, this idea causes a significant increase in the cost of the system. An interesting alternative is the use of compact and cost-effective CT spectrometers (Ocean optics, Avantes), which typically provide ~100 pm of spectral resolution for a spectral range of ~100 nm and an acquisition rate of up to 100 Hz /

kHz for a fraction of the cost of traditional spectrometers. The use of these spectrometers has recently been reported in several works [51,53,112,120].

Finally, the PR spectrometer provides the most sensitivity and fastest detection capacity (up to kHz) with simultaneous multielemental analyses when used with individual photomultiplier tubes (PMT) [24,98,99,121]. Nevertheless, the cost, size and relatively low versatility of this spectrometer limits its use in specific applications, thus this spectrometer is mainly used in industrial applications and to a lesser extent in research laboratories.

2.4 Detection in the vacuum ultraviolet (VUV) range

The possibility of accessing the VUV spectral range offers several advantages over more conventional UV-Vis-NIR regions, such as the significant improvement of the detection of certain elements such as sulfur, phosphorus, and carbon, less spectral interference with transition metals and a lower continuum emission [122,123]. Nevertheless, VUV plasma emission is hampered by air absorption restricting the measurements of oxygen-free conditions and specific optical materials. Solutions for LIBS-based imaging in the VUV range include working under vacuum conditions and having spectrometers and light collection systems purged with inert gases [121]. Different detection systems can be used: first, CT spectrometers in combination with microchannel plates with a photodiode array (MCP-PDA) and second, PR spectrometers that have been already used for VUV-LIBS analyses of steels [24]. Other specific VUV detection systems can be found in the literature, such as systems in the deep VUV range (40-160 nm) that use, for example, a near normal-incidence concave grating spectrograph [124]. Recently, our team proposed an Ar-purged detection system composed of a VUV probe coupled to a Maya2000Pro compact CT spectrometer, which performs VUV-LIBS imaging under ambient atmospheric conditions reaching an LOD of 0.2 wt% for sulfur in mine core samples [123].

2.5 Autofocus

To guarantee reproducible ablations during the entire sequence scan, it is imperative to ensure a constant distance between the focusing objective and the sample surface. This constant distance is particularly important in microscopic configurations, for which the variation of the focusing distance should not exceed a fraction of the depth of focus (i.e., ~ 10 µm). Polishing the sample surface is generally sufficient to ensure a flat scanning area for small samples; however, when analyzing large samples, it is difficult to obtain a sufficiently flat surface even after rigorous sample preparation, and an autofocus is required. Three main types of autofocus systems have been reported. J. Novotný *et al.* proposed an autofocus system based on a sharpness analysis of the sample view captured with a

complementary metal oxide semiconductor (CMOS) camera with a vertical accuracy in the range of ± 50 µm [105]. The second type, applied by C. Beresko *et al.*, is only valid for analyses carried out in pixel by pixel mode since this system is based on the direct monitoring of the LIBS signal intensity at a fixed X-Y-position. Several laser pulses are fired while adjusting the vertical position of the sample, fixing the focusing position when the LIBS signal is maximal [112]. This method is suitable for surfaces with fluctuations several millimeters in height. The operational speed and lateral resolution are poor due to the necessity of multiple laser pulses. Finally, J. O. Cáceres *et al.* proposed an autofocus system able to work in a continuous configuration at 100 Hz operating speed by analyzing the plasma shape and position collected by a fiber bundle consisting of four fibers and a fast algorithm that corrects the vertical position (accuracy of ± 5 µm) in real time [56].

2.6 Coupling with other techniques

The all-optical and rather simple instrumentation of LIBS imaging systems make it easy to directly couple with other compatible techniques. It is relatively straightforward to visualize and capture an optical image of the sample surface with a conventional CCD camera, which allows for the optimization of the ablation focusing and sample positioning [69,81,85,100,105,120]. The possibility of stacking elemental and optical images for direct comparison is of paramount importance in applications such as medical diagnoses to obtain complementary elemental information. S. Moncayo *et al.* reported multielemental LIBS-based images of human paraffin-embedded skin samples over the entire biopsy scale in a way that was complementary and compatible with microscope histopathological examination [125]. The combination of LIBS and Raman is also well known; both laser-based analytical techniques share part of their instrumentation and can be integrated for studying the molecular and elementary fingerprint of a surface, supplying new sample information. The results of this combination in earlier LIBS-based imaging studies have been shown by M. Hoehse *et al.*, who proposed the use of a two-laser LIBS–Raman automated microanalysis system equipped with a newly designed dual arm Echelle spectrometer to characterize an iron ore sample [117]. Additionally, LIBS combined with laser-induced fluorescence (LIF) is a promising approach to improve the LOD. In LIBS-LIF, a second laser tuned to a specific wavelength is directed to the LIBS plasma plume and used for re-excitation, inducing a fluorescence signal. This combination has been investigated by J. Li *et al.*, who demonstrated optimal locations for re-excitation in plasmas induced on steel samples [119]. Finally, LIBS has also been coupled to techniques that are not fully optical-based such as LA-ICP-MS. Both techniques have identical laser sampling processes that enable simultaneous application. A tandem LA/LIBS instrument has been developed and applied by the group of R. Russo to various applications fields [76,78,80,95].

3. Data processing

Like other hyperspectral techniques, LIBS-based imaging suffers from the bottleneck of data processing; several millions of spectra can be measured daily, becoming a real challenge for data set analyses [104]. Considering the growing speed of analysis up to 100 Hz, the complexity of emission spectra with hundreds or thousands of emission lines, and the presence of spectral interference, data processing requires more sophisticated extraction approaches to streamline the process. Despite the importance of data processing, very little is found in the literature regarding data processing of LIBS-based imaging. Different approaches for performing intensity extraction, semi-quantitative elemental images and the use of chemometric methods are reviewed in the following sections.

3.1 Intensity extraction

Most literature reports regarding LIBS-based imaging results have been obtained using simple samples, where the objective was to image trace or detect minor elements in a homogeneous matrix. In this type of sample, it is relatively easy to process the average spectrum of the whole dataset and identify the main emission lines of the elements of interest. One procedure for data extraction was proposed by L. Bassel *et al.* where a calcium carbonate ($CaCO_3$) speleothem was scanned to study the spatial distribution of trace elements such as Mg, Si, and Al (c.f. figure 3) [118]. In this approach, the line intensity is retrieved for each sampling position by defining a baseline and subtracting the baseline from the emission signal. A two-dimensional matrix containing the line intensity at each position of the sample is obtained and can be displayed using a false-color scale in the form of elemental images. Another interesting methodology was proposed by M. Abdelhamid *et al.* [109]. In that method, only those peaks that supersede a signal-to-noise ratio of 3 were considered for data extraction.

In contrast, when samples contain several phases and different matrixes, data analysis becomes much more challenging. Such multiphase analysis is particularly difficult when one or several phases are associated with elements that present complex spectral structures, such as iron (Fe) and titanium (Ti). In such cases, selecting an appropriate spectral line requires the analyst's expertise and a rigorous case-by-case evaluation of the spectral dataset. To facilitate the analysis, one possibility is to consider each phase as an independent sample [126]. For each phase, the strategy is to first to define a binary mask image using, for example, the major lines associated with the corresponding matrixes. Second, considering the mask image, all of the LIBS spectra associated with a given phase can be extracted and averaged, which allows for independent averaged spectra, one per matrix contained in

the sample. From this procedure, it is then possible to use the conventional approach, thus eliminating any possible risk of spectral interference from other phases.

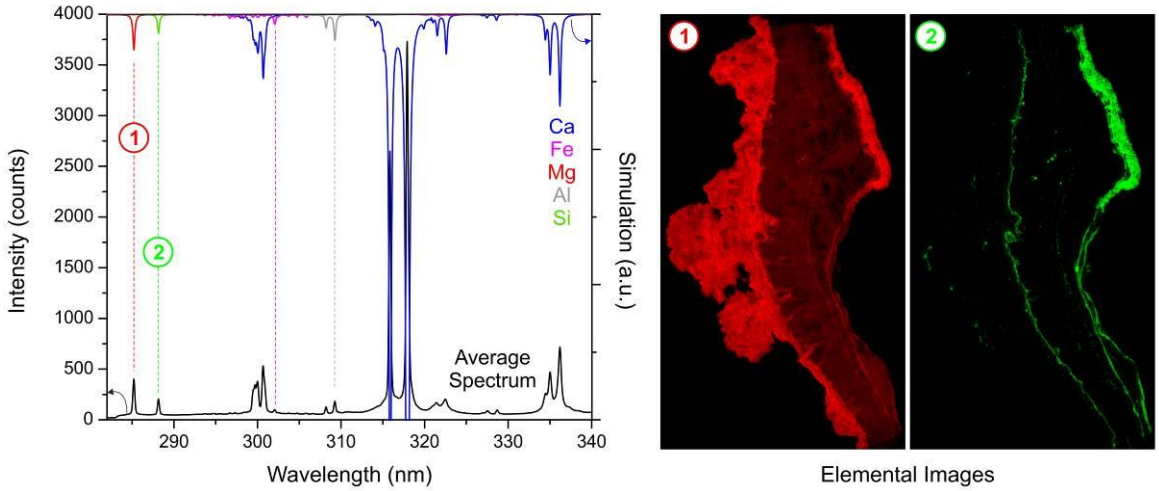

Fig. 3. Example of data processing using the average spectrum [118].

3.2 Quantification

In LIBS-based imaging experiments, the term "quantification" may be excessive. The destructive nature of laser ablation generally does not allow for averaging of several measurements at one sample position and therefore, a quantification strategy must be deployed without using any statistical information [127]. Many works have reported "semi-quantitative" mapping of various types of samples. The most common calibration method transforms the relative-abundance images into quantitative-abundance images after referring to the calibration measurements performed on the standard samples. The instrumental accuracy may only be obtained on homogeneous standards. This procedure has been used for the quantitative mapping of boron-doped crystalline silicon [77], steel [119], biological organs [128], glass [78,85] and other types of materials [78,90,97]. When reference samples are not available or simply do not exist, one possibility is to consider the mapping measurement as representative of whole sample volume. The bulk concentration can be obtained by other analytical techniques, such as ICP-based or X-ray fluorescence (XRF) analyses, and then be used to calibrate the mapping experiments. In such a way, semi-quantitative maps of Ti-doped sapphire [129], murine kidney [113], and heterogeneous catalyst [130] have already been reported. In other cases, spatially resolved methods can also be used to calibrate LIBS measurement. F. Trichard *et al.* used line profiles performed with an electron microprobe on a catalyst section to calibrate the LIBS image of palladium (Pd) [131]. In this work, several lines of Pd with various intensities were used to exploit the highest dynamical range without being affected by self-absorption. L. Krajcarová *et al.* reported the use of LA-ICP-MS analysis at different positions to calibrate the LIBS maps in plant samples [107].

3.3 Chemometric methods

In LIBS-based imaging, the large datasets and the complexity of samples can encourage the implementation of chemometric tools for data processing. The hyperspectral analysis of large LIBS datasets has extensive computational requirements: principal component analysis (PCA) and partial least squares (PLS) are the most widespread chemometric methods because of their simplicity and good throughput for qualitative and quantitative analyses, respectively.

PCA is one of the most powerful unsupervised tools for data processing. PCA allows for reduction of the dimensionality by the linear combination of the data's original variables **X** by defining a new set of variables (PCs) that retain the meaningful information. In brief, the final result of a LIBS-based image experiment is a hyperspectral data cube composed of two spatial dimensions, x and y, corresponding to the map coordinates and one spectral dimension (λ), where each cell of the cube represents the intensity of an emission line from a single-shot spectrum. After unfolding, PCA is applied to the **X** matrix (x*y, λ), obtaining the score (**T**) and loading (**P**) matrixes. Each PC is refolded, generating the score image and allowing for qualitative study of the distribution of the elements defined by the loading vector. In experiments where the number of spectra is not extensively large, it is possible to process a PCA model on the complete dataset. R. Carvalho *et al.* applied hyperspectral LIBS imaging with PCA to investigate the metal composition of a printed circuit board (PCB). The strategy was to apply a first PCA model on the complete dataset, sized 12,000 × 12,288 (locations × spectral variables), retrieving the most intense lines observed at the first loading vector, and apply a second PCA on only the 18 selected lines (12,000 x 18), obtaining the corresponding scores and loading values, which allows for the detection of precious and toxic elements in PCB samples [61]. The same strategy was followed by M. A. Sperança *et al.* for the investigation of coprolite and fossil samples. The hyperspectral cube is unfolded and normalized and a PCA is applied to the complete dataset, sized 780 × 12,288, retrieving the elements that contributed most to the sample characterization [66]. The data are auto scaled (mean equal to zero and standard deviation equal to 1), and a new PCA is calculated for each pulse and evaluation of the score maps. When the dataset is large, the calculations of PCA require high computing power not accessible in an office computer. Nevertheless, there are different strategies that can be applied to reduce the computing requirements such as binning the wavelengths, reducing the spectral range, and/or processing only a certain percentage of spectra and then building up the PCA model for all spectra. This last strategy was applied by J. Klus *et al.* as they processed a reduced data matrix (2500 × 26000), obtaining a new system of coordinates, and then, the whole data set (22500 × 26000) is predicted by obtaining a new scores matrix [106]. Finally, S. Moncayo *et al.* applied PCA analysis for the multivariate hyperspectral

analysis of a megapixel LIBS image (~2 million × 2048) as a new data processing methodology. PCA is applied to analyze a mineral turquoise sample using a computer server (RAM > 256 GB), although similar results and conclusions were found with an office computer after applying strategies to reduce the computer requirements. PCA was demonstrated to be a powerful tool capable of identifying the main mineral phase of the sample. PCA is also useful for detecting experimental issues and artifacts (such as matrix effects and saturation); PCA allows for identification of isolated pixels associated with one or several elements. More importantly, PCA improves data extraction by obtaining mask images associated with the main phases [58].

On the other hand, PLS relates the **X** and the **Y** (concentrations as responses) matrixes, establishing a calibration model. The concentration of a new set of samples is then predicted. PLS has been applied to analyzing LIBS-based images for the prediction of semi-quantitative chemical maps of different types of samples. To calibrate the models, a set of LIBS spectra are used as the **X** matrix, and the reference response is usually obtained by bulk analysis with other techniques or by using reference materials. After the calibration, the concentrations of spatially resolved data sets are predicted and transformed into semi-quantitative element maps. This methodology has been applied, for instance, in the food industry [64,71,90] for the analysis of the calcium in infant formula, the content of copper in meat, and the sodium and potassium in beef using pellet samples. The use of pellets improves the homogeneity and reduces the matrix effect, which is a good strategy when a "bulk" analysis is desired; however, the spatial information is lost. PLS regression has also been applied to the analysis of heterogeneous samples without any preparation, as shown in the works of C. D. Quarles *et al.* [76] and K. Kuhn *et al.* [132]. The first study analyzed the fluorine content on a small area (16 mm^2) of a rare earth element (REE)-rich mineral, comparing the accuracy and precision of the PLS model with univariate analysis. The second example used PLS to obtain the element distribution of several metals as well as phases or mineral distributions of drill core samples at larger scales (1 meter and 5 cm in diameter). All these studies demonstrate that PLS regression can improve the quantitative univariate results but also indicate that matrix effects are its main limitation.

Another approach based on self-organizing maps (SOM) has been recently developed both for the qualitative identification of the mineralogical composition of a wall painting fragment [104] and the characterization of uranium in sandstone-hosted uranium ores [106]. The SOM algorithm uses as inputs the intensities main emission lines of the elements in the sample and assigns each spectrum to the closest neuron, in a competitive way. The coordinates (elements considered) of winning neurons provide the average composition of the spectra within the cluster allowing the characterization and discrimination among mineral phases. More recently, the group of V. Pallesci applied SOM coupled with CF-LIBS in order to provide a quantitative map such sample [133]. In this context, the spectra assigned to each cluster were averaged and their corresponding elemental composition were

obtained by CF-LIBS. Although not able to assess the fine compositional variations inside the different cluster, this approach reproduces well the texture of the samples with a reasonable precision of about ± 1% on the major elements and proportionally higher on the minor and trace elements.

4. LIBS imaging applications

4.1 Geomaterials

4.1.1 Paleoclimate studies

To develop a rich understanding of past, present and future climates and their environmental impacts, accurate analytical methods capable of analyzing a wide range of geological samples with different morphologies, ages and provenances are firmly required. Such analysis remains a major challenge from a technical point view, mainly because of the diversity in samples. LIBS-based imaging studies have provided important information in the field of Earth science, showing its potential to characterize climate proxies in paleoclimate investigations. This research topic has been largely explored by the LIBS community, and we focus only on the most recent works. To distinguish between species generated in dry or wet climate periods, M. Wang *et al.* [50] carried out a LIBS-based imaging analysis on carbonate rocks to study the geochemical content by analyzing the Mg/Ca and Sr/Ca ratios. T. Xu *et al.* performed similar experiments in carbonates, clays and silicates to show the elemental distribution of various elements (Si, Al, Fe, Ca, Mg, Na and K) in shale pellets [69]. Their results provided evidence regarding the depositional environments and the sedimentary processes. In the context of planetary exploration, crucial information could be obtained from volcanic Martian analog basaltic rocks. As a proof of concept, in Mars-simulated conditions, C. Lefebvre *et al.* identified various mineral depositions by the elemental intensity ratios in a 3D LIBS configuration [114]. A recent study of N. Hausmann *et al.* showed consistent changes in the Mg/Ca elemental ratios of marine mollusk shells observed on LIBS maps with an LOD of approximately 100 ppm [65]. An article recently published by M.A. Sperança *et al.* studied coprolite and fossil samples within geological periods from the Permian to the Oligo-Miocene to determine the diet and interaction with the environment of extinct animal species by analyzing their P and Ca contents [66]. Finally, the possibility of imaging large-scale speleothems and coral samples has been demonstrated by J.O. Cáceres *et al.*: in this work, the authors measured sections of approximately 20 cm^2 with a lateral resolution of 15 µm and estimated LODs in the range of 10 ppm on a speleothem and a coral skeleton, which resulted in megapixel elemental images (c.f. figure 4a). Their findings for the Mg, Sr, Fe, Mn, Al and Si contents revealed laminar structures related to vegetation and climatic variations throughout the years [56].

4.1.2 Mineralogy

Similar to paleoclimate applications, LIBS-based imaging has also provided important information in the study of minerals and rocks. Several studies have examined chemical heterogeneities of mineral samples to assess their elemental quantification, to classify minerals and to establish their origin and provenance. Studies in recent years have provided important information regarding the characterization of rare earth element (REE) contents in ores. J. R. Chirinos *et al.* used a tandem LIBS / LA-ICP-MS instrument to detect Ce, La, and Nd in 3D compositional mapping and their isotopes, covering sample surfaces sized < 1 mm² [95]. More recently, S. Romppanen *et al.* investigated the yttrium and several REE contents in various minerals on sample surfaces sized several cm² [100]. Fluorine has also been detected in a Bastnäsite rock with an LOD of 135 ppm [76], and more recently in pellets [93]. Light elements (Z < 6) such as Li, Be, and B, have been measured on petrographical hydrothermally altered spodumenes (Li-pyroxene) and other minerals such as petalite or eucryptite with an estimated LOD of approximately 240 ppm for Li [85].

A considerable amount of literature has also been published in the mining industry field. Characterizing the spatial distribution of elements in ores provides clues to the sources of the ore and the deposition processes. These data assist in the decisions for further prospects in the field and the evaluation of the economic viability for ore extraction and refining. M. Hoehse *et al.* examined heterogeneous chromium ores slabs from Norway to study the distributions of Cr and Mg in the forsterite phase ($MgSiO_4$) [117]. The spatial distribution of Pb and S in the galena phase (PbS) was analyzed by J. Novotný *et al.* in chalcopyrite stones (c.f. figure 4b) [105]. B. Connors *et al.* performed on-site analyses of sulfide minerals in different rich-gold rocks [52]. Mine waste drill cores were investigated to identify metal enrichment and variability in lithological zones [132]. More recently, the contents of S, B, and As on a Canadian mine core composed of several mineral phases was explored by F. Trichard *et al.* [123]. The compositions of drill cores were also investigated by K. Rifai *et al.*, with special emphasis on the gold content [72]. Space-resolved LIBS has been applied to the characterization of cave walls, demonstrating the migrations of certain elements between coralloids and bedrocks [118]. In addition, the capability of LIBS-based imaging to obtain megapixels has been explored by S. Moncayo *et al.* and C. Fabre *et al.* The first work analyzed a turquoise sample, providing the elemental compositions of Al, Fe, P, Cu and Si [58]. The second work, by C. Fabre *et al*., analyzed a complex multiphase hydrothermal ore sample, identifying five different mineral phases on a 5 cm² sample surface [126]. Minor and trace substituent elements as well as REE (La, Y), were detected at the ppm scale and mapped on the 15 µm resolution LIBS images of more than 2 million spectra, allowing authors to obtain the signature of the ore source and deposition processes.

4.1.3 Archeology

Space-resolved LIBS analysis provides the means to understand and characterize archeological samples including buildings, monuments and objects of all sizes, comprising a great variety of materials. LIBS-based imaging has been demonstrated to be of great interest in a wide range of archaeological applications such as authenticity and provenance studies and diagnostics and characterization of artifacts for their conservation. There is one essential difference between modern and ancient material analyses in that an art object cannot be replaced. This fact necessitates a great amount of technological innovation that eventually boosted the development of the technique. Submillimeter spatial resolution characterization of artifacts was reported in the study of B. D. Strycker *et al.* [102] on buried objects and in the work of C. Beresko *et al.*, conducting 3D mapping with a 1 mm Z-dimension to reveal the spatial distributions of Na, Fe, and Pb [111]. S. Pagnotta *et al.* investigated the state of conservation and production techniques of ancient mortars by using 2D multi-elemental mapping of Na, Mg, Al, Si, K, Ca, Ti Mn, and Fe [104]. More recently, O. Syta *et al.* identified the archeological origin of medieval Nubian murals by analyzing the elemental composition of blue painted layers. The elemental distribution of Cu and Na allowed the researchers to clearly distinguish between Egyptian blue and lapis lazuli pigments. In the same work, other elements such as Al, Si, Ca, C and O were analyzed with LODs in the range of 10 µg/g, allowing the archeologists to date and identify the city provenance (Faras, Dongola, and Banganarti) in ancient artifacts based on the production techniques used that reflect changes in their elemental distributions [97].

4.1.4 Cement and Concrete

The field of civil engineering also requires the application of spatially resolved analyses in applications such as cement and concrete surface analysis. LIBS-based imaging has been demonstrated to be an alternative strategy that enables the elemental analyses of reinforced concretes and mortars. It is widely known that reinforced concrete structures seriously deteriorate due to chloride attack [134]. B. Šavija *et al.* applied LIBS elemental images to determine the distributions of chloride on different types of reinforced concretes, covering a surface of 200 cm^2 to provide insight into the mechanisms of deterioration. Multielemental analysis of chloride with Na, C, Ca, O, Fe distributions allowed the researchers to understand the influence of mechanical cracks on chloride ingress to prevent concrete deterioration [88]. S. Hong *et al.* performed a similar study, investigating the 3D distribution of chloride and comparing their findings with those of a more conventional geophysical method, i.e., ground penetration radar analysis. The researchers found a good correlation between both techniques [135]. More recently, the potential of LIBS to discretize

phase boundaries inside heterogeneous mortars and concretes has been evaluated by C. Gottlieb *et al.*; an example of the reported images is presented in figure 4c [120].

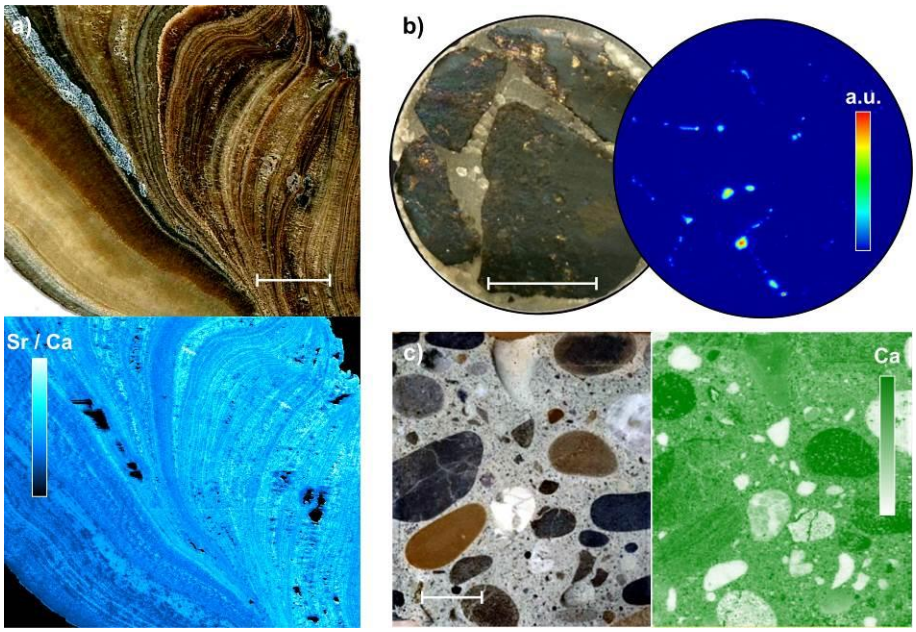

Fig. 4. Optical images and corresponding LIBS elemental images for different geomaterials. a) Speleothem section of a 5 x 4 cm surface and the related 15-µm resolution image of Sr normalized by Ca, revealing a laminar structure [56]. b) Chalcopyrite stone 25 mm in diameter and the respective chemical image of Pb, representing galena veins (PbS) across the cut [105]. c) Concrete section of a 5 x 4 cm surface and the corresponding Ca distribution image, allowing for the identification of aggregates [120]. The scale bars represent 1 cm.

4.2 Industry

4.2.1 Metallurgy

The chemical compositions of iron and steel products define their physical properties with a very close tolerance. LIBS-based imaging has been largely explored in the iron and steel industry for the composition control of both raw materials and complex pieces, ensuring the operational and commercial purposes of these materials. I. Lopez-Quintas *et al.* reported 3D elemental images of Fe, Cr, Ni and Mn to assess the compositional differences in volume of a complex heterogeneous engine valve [94]. The influence of surface roughness on different stainless steels by LIBS-based imaging was also evaluated by the same group [136]. Additionally, F. Boué-Bigne *et al.* demonstrated the possibility of using LIBS as a method complementary to human-perception in the study of cementite network boundaries by analyzing high carbon steel products in two consecutive works [98,99]. More recently, U. A. Taparli *et al.* performed in-situ measurement of the heat affected zone during

tungsten-inert-gas (TIG) welding processes on austenitic stainless steels. The elemental repartition allowed them to understand the process and resolve the defects in the weld pool during the solidification process [137]. Certain applications also require spatially resolved analysis, as for sorting metallic materials in recycling and recovering precious or hazardous pieces. R. Carvalho *et al.* evaluated the compositions of small size components present on printed circuit boards (PCB), demonstrating multielemental detection of Al, Au,Ba, Ca, Co, Cu, Fe, K, Li, Mg, Mn, Na, Ni, Sb, Si, Sn, Ti and Zn [61]. Another interesting and challenging application is the analysis of hardfacing alloys, which are alloys on which a coating of hard material has been deposed by welding or joining to improve its wear properties. J. A. Varela *et al.* succeeded in observing the partial dilution of tungsten carbide spheres in hard coatings with different concentrations by conducting both W analysis in 2D mapping and depth profiling [91]. J. Li *et al.* analyzed 22 steel samples using LIBS and LIBS-LIF, performing Cr, Ni and Fe mapping on 6 mm^2 sections [119]. Other alloys and metallic materials have also been analyzed by LIBS-based imaging. The dealloying process of brass pieces in 3D experiments demonstrated a decrease of Zn intensity near the surface [70]. V. N. Lednev *et al.* proposed the multielemental analysis of nickel alloys reinforced with tungsten carbide, showing the distributions of Ni, Fe, Cr, Si, W, Co and C [55]. The characterization of thin layers has also been investigated to evaluate the compositions of thin films of copper on glass and thin films of yttrium, barium, and copper oxide on MgO substrate [63]. An example of the results reported in this reference is shown in figure 5a.

4.2.2 Batteries, semiconductors and crystals

LIBS-based imaging has also been applied in the electronic and semiconductor fields for the evaluation of component performance and to improve the production processes. Li-ion batteries were investigated in two recent works. First, H. Hou *et al.* analyzed the distribution of several atomic ratios of major and minor elements in a solid electrolyte matrix under different conditions. Authors reported the presence of impurities, compositional changes, and gradients in Li/La, Zr/La, and Al/La ratios (c.f. figure 5b) [83]. Second, P. Smyrek *et al.* explored the complementarity of LIBS mapping combined with depth-profiling techniques to develop a new battery cell architecture design by analyzing the Li-ion diffusion kinetics within the cathode [89]. S. Imashuku *et al.* reported a poorly resolved but quantitative repartition of Li on a $LiCoO_2$ cathode by using standard analysis by ICP [138]. The characterization of semiconductors and crystals has also been a matter of ongoing research. S. Darwiche *et al.* analyzed elemental impurities in different solid silicon substrates for a deeper understanding of production processes of photovoltaic grade silicon [77]. The authors made an original contribution, reporting the distribution of a boron dopant with an LOD of approximately

2.10^{-4} mg/g. The findings of J. Li *et al.* revealed the dopant distribution in Yb-doped fiber [82]. In another work, the purpose of E. Kim and H. Lim was to determine and visualize the Zn content in SiO_2 fibers to develop electronic polycarbonate conducting polymers [139]. These results showed significant heterogeneities in the Ca and Si distributions and no correlation between Zn and Si. Then, P. Škarková *et al.* focused on determining the Cd toxicity and bioaccumulation in aquatic plants dissolved from Cd-based quantum dots at different pH, even in nanoparticles with no visible luminescence [140]. A study of B. Wiggins *et al.* presented 2D millimetric mapping of Li, In, Se, Na, Ca, K in Li In Se_2 crystals using a multielemental approach to identify inclusions [84]. Finally, the titanium distributions in Ti-doped sapphires grown by Czochralski and Kyropoulos techniques have been analyzed by G. Alombert-Goget *et al.*, showing different radial profiles of Ti^{4+}. These results provide valuable insight into controlling the growth process to increase the quality of Ti:sapphire materials [129].

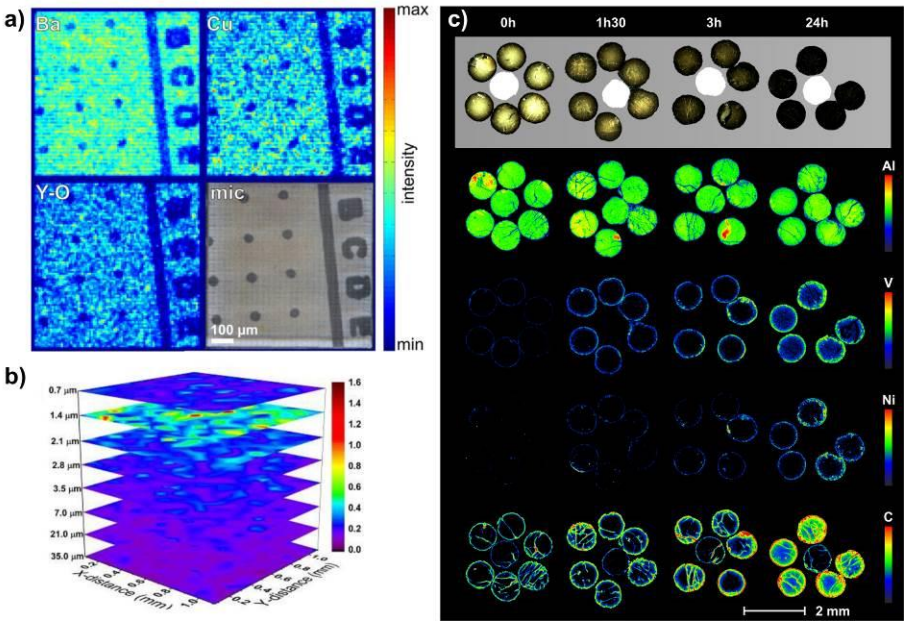

Fig. 5. LIBS elemental images for different industrial samples. a) 6-µm resolution fs-LIBS images of Ba, Cu and Y-O diatomic molecular emissions from a micropatterned YBCO thin film on a MgO substrate section of 800 x 800 µm² surface [63]. b) Layer-by-layer LIBS elemental images of the Al/La atomic ratio of a solid-state lithium-ion LLZO electrolyte prepared under specific conditions (6 hours of annealing) [83]. c) Optical images of alumina refining catalyst supports impregnated by asphaltenes under different conditions and the corresponding 30-µm resolution LIBS images of the Al matrix and the V, Ni, and C distribution maps [130].

4.2.3 Catalysis

The petroleum industry and especially researchers focused on solid heterogeneous refining catalysts require techniques able to provide the elemental distributions of active elements or poisons to increase the catalyst performance. Light elements such as S and C cannot be easily detected with the commonly used EPMA at the same speed. Since it was first reported in 1999 by the group of J. Laserna, the analysis of catalysts has been explored in several LIBS-based imaging works [37,40–42], [131], [130]. In general, the use of LIBS offers faster analysis directly under atmospheric pressure with quantification limits 60 times lower than those of EPMA. Our group recently published three papers evaluating the application of LIBS-based imaging in the petroleum industry. First, we studied the distribution of Pd within typical alumina catalysts, demonstrating the quantification capability of LIBS over a large dynamic range from the % to the ppm scale with an LOD of 18 ppm for Pd in a single-shot configuration [131]. These results were then used to estimate the catalyst crust thickness (related to the apparent activity) by a methodology derived from conventional EPMA analysis [141]. Our last paper regarding this topic analyzed the internal diffusion of asphaltenes in mesoporous alumina catalysts supports. We showed the micrometer spatial distributions of S, Ni, V, C and Al (c.f. figure 5c), and proposed a new methodology to study the transport and reactivity in catalysis, aiming to enhance the design of reactivity models at the pellet scale [130].

4.2.4 Nuclear Field

The advantages of performing remote and in-situ analysis under dangerous environments make LIBS-based imaging a suitable technique for analyzing nuclear materials. C. Li *et al.* reported two studies conducted for the Experimental Advanced Superconducting Tokamak (EAST) magnetic fusion energy reactor. The first study focused on the 2D distribution and depth profiling of Li deposition in plasma-facing materials [74] and the second to studied the distributions of impurities (H, O, Ar, K, Na, and Ca) of a co-deposition layer of Li-W used in the reactor walls [59]. X. Wang *et al.* investigated the fractionation long term behavior of Mo, Ca, Sr, Al, Fe and Zr and rare-earth elements such as Eu, Nd, Pr and La on a Mo-rich nuclear waste glass-ceramic [81]. Recently, researchers have shown an increased interest in studying the U distributions in geological materials. J. Klus *et al*. reported U distributions in sandstone ores with an estimated LOD of 0.26 %wt. [106]. Finally, B. T. Manard *et al.* performed LA-ICP-MS and LIBS in tandem to map and characterize U particles at concentrations down to 0.01% in a mixed powder of U oxide and iron/nickel with potential application for nuclear forensics and materials safeguards [78].

4.3 Biomedical

Biomedical applications appear to be one of the most promising fields for the development of LIBS-based imaging. The capability of LIBS to obtain in situ multielemental (endogenous or exogenous) tissue images has received increased attention. Several reviews regarding the application of conventional LIBS analysis of biological specimens have already been published [142–146] and therefore, we only describe the latest published works.

4.3.1 Biology: preclinical evaluation of metal-based nanoparticles

Our group has previously demonstrated the biodistribution of nanoparticles (NPs) in murine kidneys, aiming to analyze trace elements in biological tissues at microscopic spatial resolution for routine elementary investigations [43,44]. Several articles have followed the technical evolution, reporting the most important improvements of this methodology (c.f. figure 6a) [44,128,147]. Currently, the technique allows for different types of soft material analysis such as multielemental 3-D images, either by volume reconstruction or in-depth analysis (c.f. figure 6b) [113], working in a complementary way with conventional imaging techniques, i.e., transmission electron microscopy and fluorescence microscopy [73], studying the distribution of gold-based NPs in various organs such as the kidney, liver and spleen [148] and assessing the biodistribution of endogenous metals trapped in modified NPs [149]. The mechanisms of tumor targeting have also been recently investigated as shown by A. Detappe *et al.* and S. Kunjachan *et al.* in Gd-based and Au-based NP tumor penetration, respectively [150,151].

4.3.2 Medical: assistance with diagnosis

The complementarity of LIBS-based imaging with routine histopathological analysis may assist in producing a rapid and accurate diagnosis. This technique is especially suitable when foreign substances contained in human specimens are found by the pathologist, which in some cases may lead to misdiagnosis or insufficient diagnosis. So far, very little research has been carried out and only a small number of works have been published. The large majority of human biopsies are stored in paraffin; S. Moncayo *et al.* reported the proof of concept of complementarity LIBS-based imaging and conventional histopathology by analyzing endogenous elements in paraffin-embedded skin biopsies [125]. B. Busser *et al*. also identified exogenous metals such as W, Ti, Al or Cu in a granuloma, a pseudolyphoma and skin biopsies containing foreign pigments [75]. Finally, M. Bonta *et al.* proposed the combination of both LIBS and LA-ICP-MS techniques for the analysis of malignant pleural mesothelioma samples, aiming at extending LIBS detection capabilities [79,80].

4.3.3 Vegetal materials

As discussed above, several reviews have addressed space-resolved LIBS applications on vegetal samples [142–144]. The most recent applications, mainly presented by the group of Kaiser, have focused on studying the absorption of metals and their transport in plants. L. Krajcarová *et al.* showed the distribution and accumulation of copper in stems [107] and silver NPs in roots [54]. Further analysis of cadmium toxicity and accumulation were reported by P. Modlitbová *et al.* [108]. Finally, the absorption and diffusion of pesticides in plant were reported by C. Zhao *et al.* in 2D and 3D analyses [53]. There is a recognized need for developing methods to study the distribution and accumulation of micro- and macronutrients for direct, rapid plant nutrition diagnosis. M. B. Bueno Guerra *et al.* proposed the direct analysis of dried sugar cane by energy dispersive X-ray fluorescence (EDXRF) and LIBS-based imaging to determine the microchemical distributions of P, K, Ca, Mg, Fe, Cu, Mn, Zn, B and Si in fresh leaves [60].

4.3.4 Forensic science

LIBS-based imaging has also been proposed as a useful tool in the field of forensic science. Forensic evidence covers a wide range of biological materials to be analyzed, and certain evidence requires specific considerations regarding its manipulation and protection to be admissible in court. A search of the literature revealed few studies regarding the use of LIBS in forensic applications. M. López-López *et al.* explored a new non-destructive methodology to analyze gunshot to preserve the evidence [57]. J-H. Yang *et al.* performed compositional analysis to discriminate two overlapping fingerprints [67]. Following the fingerprint analysis, M. Abdelhamid et al. developed a new method to analyze fingerprints containing explosive residues by optical-catapulting-LIBS [109]. To elucidate the cause of death, F. J. Fortes *et al.* [62] determined the concentration of strontium in teeth. Finally, several works have been conducted regarding food authenticity and security, preventing illegal adulteration [64,71,86].

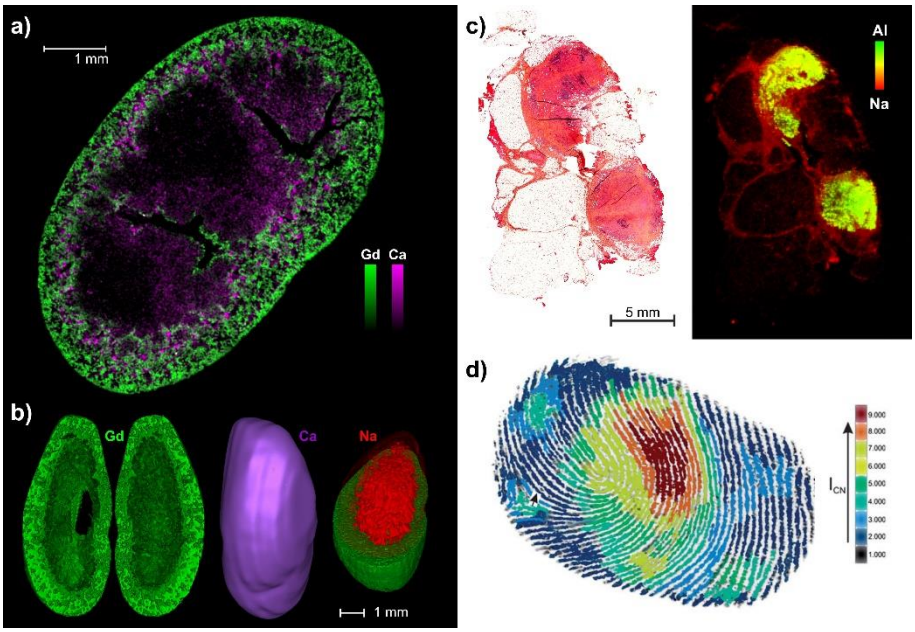

Fig. 6. Examples of LIBS elemental images obtained in the biomedical field. a) Biodistribution of Gd-based NPs in murine kidney 3 hours after their administration [113]. b) 3-dimensional representations of Gd, Ca and Na at the entire kidney scale [113]. c) Histopathologic and elemental images showing the accumulation of Al in a cutaneous granuloma [75]. d) CN image of a fingerprint obtained with optical-catapulting-LIBS [109].

5. Conclusion

In recent years, LIBS-based imaging has seen remarkable development in terms of both instrumentation and applications. This approach is indeed extremely versatile and simple to implement in comparison with other space-resolved elemental techniques. The analytical performances of this technique are obviously dependent on the experimental configurations used (type of laser focusing, spectrometers, and detectors); however, several works have demonstrated the possibility of reaching ppm-scale sensitivity with microscopic-scale resolution while ensuring a fast acquisition rate (100 Hz or above). Such performances are very interesting from an application point of view, and there is no doubt that LIBS imaging will continue to grow and extend in capabilities.

Therefore, with regard to the recent progress of this method, elemental imaging may represent one of the major axes of the future development of LIBS. Among the various reported applications, biomedical applications can certainly be considered to be the showcase of this technology. There are

so far two fields that have been explored in this domain; the preclinical evaluation of metal-based nanoparticles and the characterization of human specimens for helping medical diagnoses. There are, however, numerous other applications that may represent good opportunities for the LIBS community to progress and be promoted by the biomedical domain.

Despites the numerous advantages of LIBS-based imaging, there are still some technological barriers to overcome. In particular, the analysis of complex materials (i.e., composed of several matrixes) still appears to be challenging both in quantification and data processing. Further studies dedicated to these issues need to be conducted, and the use of calibration-free LIBS and advanced chemometric tools represent interesting opportunities.

Acknowledgements

This work was partially supported by Pulsalys (#L0978-L1294), the French region Rhônes Alpes Auvergne (Optolyse, CPER2016), and the French ANR (projects MediLIBS and Imazinc). In addition, we gratefully acknowledge Dr. Frédéric Pelascini from the Cétim Grand Est, Dr. Florian Trichard from Ablatom, and Professor Christophe Dujardin from ILM for fruitful discussions.

6. References

[1] D.A. Cremers, L.J. Radziemski, Handbook of Laser-Induced Breakdown Spectroscopy, Wiley & Sons, Ltd, New-York, 2006.

[2] Miziolek W. A., V. Palleschi, Schechter I., Laser-Induced Breakdown Spectroscopy (LIBS), 1st ed., Cambridge University Press, 2008.

[3] D.W. Hahn, N. Omenetto, Laser-Induced Breakdown Spectroscopy (LIBS), Part I: Review of Basic Diagnostics and Plasma-Particle Interactions: Still-Challenging Issues Within the Analytical Plasma Community, Appl. Spectrosc. 64 (2010) 335–366.

[4] D.W. Hahn, N. Omenetto, Laser-induced breakdown spectroscopy (LIBS), part II, Appl. Spectrosc. 66 (2012) 347–419.

[5] D.A. Cremers, L.J. Radziemski, Handbook of Laser-Induced Breakdown Spectroscopy, Second Edition, John Wiley & Sons, Ltd, 2013.

[6] Brech F., Cross L., Optical micro-emission stimulated by a ruby laser, Appl. Spectrosc. 16 (1962) 59.
[7] Debras-Guédon J., Liodec N., De l'utilisation du faisceau d'un amplificateur à ondes lumineuses par émission induite du rayonnement (laser à rubis) comme source énergétique pour l'excitation des spectres d'émission des éléments, C.R. Acad. Sci. 257 (1963) 3336–3339.
[8] St Onge L, Detalle V., Sabsabi M., Enhanced laser-induced breakdown spectroscopy using the combination of fourth-harmonic and fundamental Nd:YAG laser pulses, Spectrochim. Acta Part B 57 (2002) 121–135.
[9] K.Y. Yamamoto, D.A. Cremers, M.J. Ferris, L.E. Foster, Detection of Metals in the Environment Using a Portable Laser-Induced Breakdown Spectroscopy Instrument, Appl. Spectrosc. 50 (1996) 222–233.
[10] X. Mao, A.A. Bol'shakov, D.L. Perry, O. Sorkhabi, R.E. Russo, Laser Ablation Molecular Isotopic Spectrometry, Spectrochim. Acta Part B 66 (2011) 604–609.
[11] R.E. Russo, A.A. Bol'shakov, X. Mao, C.P. McKay, D.L. Perry, O. Sorkhabi, Laser Ablation Molecular Isotopic Spectrometry, Spectrochim. Acta Part B 66 (2011) 99–104.
[12] P. Purohit, F.J. Fortes, J.J. Laserna, Spectral Identification in the Attogram Regime through Laser-Induced Emission of Single Optically Trapped Nanoparticles in Air, Angewandte Chemie 56 (2017) 14178–14182.
[13] A. de Giacomo, R. Gaudiuso, C. Koral, M. Dell'Aglio, O. de Pascale, Nanoparticle-Enhanced Laser-Induced Breakdown Spectroscopy of Metallic Samples, Anal. Chem. 85 (2013) 10180–10187.
[14] C. Zhao, D. Dong, Comment on "Nanoparticle Enhanced Laser-Induced Breakdown Spectroscopy for Microdrop Analysis at subppm Level": Several Issues to Consider When Quantitatively Measuring Fluids Using Nanoparticle-Enhanced Laser-Induced Breakdown Spectroscopy, Anal. Chem. 88 (2016) 9869–9870.
[15] M. Dell'Aglio, R. Alrifai, A. de Giacomo, Nanoparticle Enhanced Laser Induced Breakdown Spectroscopy (NELIBS), a first review, Spectrochim. Acta Part B 148 (2018) 105–112.
[16] A. Ciucci, M. Corsi, V. Palleschi, S. Rastelli, A. Salvetti, E. Tognoni, New Procedure for Quantitative Elemental Analysis by Laser-Induced Plasma Spectroscopy, Appl. Spectrosc. 53 (2016) 960–964.
[17] Zhang Tianlong, Wu Shan, Tang Hong-Sheng, Wang Kang, Duan Yi-Xiang, Li Hua, Progress of Chemometrics in Laser-induced Breakdown Spectroscopy Analysis, Chinese Journal of Analytical Chemistry 43 (2015) 939–948.
[18] P. Pořízka, J. Klus, E. Képeš, D. Prochazka, D.W. Hahn, J. Kaiser, On the utilization of principal component analysis in laser-induced breakdown spectroscopy data analysis, a review, Spectrochim. Acta Part B 148 (2018) 65–82.
[19] T. Zhang, H. Tang, H. Li, Chemometrics in laser-induced breakdown spectroscopy, Journal of Chemometrics 2 (2018) 1-18.
[20] N.L. Lanza, R.C. Wiens, S.M. Clegg, A.M. Ollila, S.D. Humphries, H.E. Newsom, J.E. Barefield, Calibrating the ChemCam laser-induced breakdown spectroscopy instrument for carbonate minerals on Mars, Appl. Opt. 49 (2010) C211-C217.
[21] S. Maurice, S.M. Clegg, R.C. Wiens, O. Gasnault, W. Rapin, O. Forni, A. Cousin, V. Sautter, N. Mangold, L. Le Deit, M. Nachon, R.B. Anderson, N.L. Lanza, C. Fabre, V. Payré, J. Lasue, P.-Y. Meslin, R.J. Léveillé, B.L. Barraclough, P. Beck, S.C. Bender, G. Berger, J.C. Bridges, N.T. Bridges, G. Dromart, M.D. Dyar, R. Francis, J. Frydenvang, B. Gondet, B.L. Ehlmann, K.E. Herkenhoff, J.R. Johnson, Y. Langevin, M.B. Madsen, N. Melikechi, J.-L. Lacour, S. Le Mouélic, E. Lewin, H.E. Newsom, A.M. Ollila, P. Pinet, S. Schröder, J.-B. Sirven, R.L. Tokar, M.J. Toplis, C. d'Uston, D.T. Vaniman, A.R. Vasavada, ChemCam activities and discoveries during the nominal mission of the Mars Science Laboratory in Gale crater, Mars, J. Anal. At. Spectrom. 31 (2016) 863–889.

[22] M. Taschuk, I.V. Cravetchi, Y.Y. Tsui, R. Fedosejevs, Micro-LIBS, Chapter 8, in: J. P. Singh and S. N. Thakur, Laser-Induced Breakdown Spectroscopy, pp. 174–196.
[23] D. Menut, P. Fichet, J.-L. Lacour, A. Rivoallan, P. Mauchien, Micro-laser-induced breakdown spectroscopy technique, Appl. Opt. 42 (2003) 6063–6071.
[24] H. Bette, R. Noll, High speed laser-induced breakdown spectrometry for scanning microanalysis, J. Phys. D: Appl. Phys. 37 (2004) 1281–1288.
[25] R. Noll, Laser-Induced Breakdown Spectroscopy, Springer, Berlin, Heidelberg, 2012.
[26] K. Janssens, W. de Nolf, G. van der Snickt, L. Vincze, B. Vekemans, R. Terzano, F.E. Brenker, Recent trends in quantitative aspects of microscopic X-ray fluorescence analysis, Trends in Analytical Chemistry 29 (2010) 464–478.
[27] J. Garrevoet, B. Vekemans, S. Bauters, A. Demey, L. Vincze, Development and Applications of a Laboratory Micro X-ray Fluorescence (μXRF) Spectrometer Using Monochromatic Excitation for Quantitative Elemental Analysis, Anal. Chem. 87 (2015) 6544–6552.
[28] K.L. Moore, E. Lombi, F.-J. Zhao, C.R.M. Grovenor, Elemental imaging at the nanoscale: NanoSIMS and complementary techniques for element localisation in plants, Anal. bioanal. chem. 402 (2012) 3263–3273.
[29] D. Pozebon, G.L. Scheffler, V.L. Dressler, M.A.G. Nunes, Review of the applications of laser ablation inductively coupled plasma mass spectrometry (LA-ICP-MS) to the analysis of biological samples, J. Anal. At. Spectrom. 29 (2014) 2204–2228.
[30] M.J. Pushie, I.J. Pickering, M. Korbas, M.J. Hackett, G.N. George, Elemental and chemically specific X-ray fluorescence imaging of biological systems, Chem. Rev. 114 (2014) 8499–8541.
[31] Reich M., Large R., Deditius P. A., New advances in trace element geochemistry of ore minerals and accessory phases, Ore Geol. Rev. 81 (2017) 1215–1217.
[32] H.J. Häkkänen, J.E.I. Korppi-Tommola, UV-Laser Plasma Study of Elemental Distributions of Paper Coatings, Appl. Spectrosc. 49 (1995) 1721–1728.
[33] C. Geertsen, J.-L. Lacour, P. Mauchien, L. Pierrard, Evaluation of laser ablation optical emission spectrometry for microanalysis in aluminium samples, Spectrochim. Acta Part B 51 (1996) 1403–1416.
[34] J.M. Vadillo, S. Palanco, M.D. Romero, J.J. Laserna, Applications of laser-induced breakdown spectrometry (LIBS) in surface analysis, Anal. bioanal. chem. 355 (1996) 909–912.
[35] T. Kim, C.T. Lin, Y. Yoon, Compositional Mapping by Laser-Induced Breakdown Spectroscopy, J. Phys. Chem. B 102 (1998) 4284–4287.
[36] D. Romero, J.J. Laserna, Surface and tomographic distribution of carbon impurities in photonic-grade silicon using laser-induced breakdown spectrometry, J. Anal. At. Spectrom. 13 (1998) 557–560.
[37] P. Lucena, J.M. Vadillo, J.J. Laserna, Mapping of platinum group metals in automotive exhaust three-way catalysts using laser-induced breakdown spectrometry, Anal. Chem. 71 (1999) 4385–4391.
[38] D. Romero, J.J. Laserna, Multielemental chemical imaging using laser-induced breakdown spectrometry, Anal. Chem. 69 (1997) 2871–2876.
[39] D. Romero, J.J. Laserna, A microanalytical study of aluminium diffusion in photovoltaic cells using imaging-mode laser-induced breakdown spectrometry, Spectrochim. Acta Part B 55 (2000) 1241–1248.
[40] P. Lucena, J.M. Vadillo, J.J. Laserna, Compositional mapping of poisoning elements in automobile three-way catalytic converters by using laser-induced breakdown spectrometry, Appl. Spectrosc. 55 (2001) 267–272.

[41] P. Lucena, J.J. Laserna, Three-dimensional distribution analysis of platinum, palladium and rhodium in auto catalytic converters using imaging-mode laser-induced breakdown spectrometry, Spectrochim. Acta Part B 56 (2001) 177–185.
[42] P. Lucena, J.M. Vadillo, J.J. Laserna, Spatial distribution of catalytically active elements and deactivants in diesel-engine automobile converters by laser-induced plasma spectrometryElectronic Supplementary Information available, J. Anal. At. Spectrom. 17 (2002) 548–551.
[43] V. Motto-Ros, L. Sancey, Q.L. Ma, F. Lux, X.S. Bai, X.C. Wang, J. Yu, G. Panczer, O. Tillement, Mapping of native inorganic elements and injected nanoparticles in a biological organ with laser-induced plasma, Appl. Phys. Lett. 101 (2012) 223702.
[44] L. Sancey, V. Motto-Ros, B. Busser, S. Kotb, J.M. Benoit, A. Piednoir, F. Lux, O. Tillement, G. Panczer, J. Yu, Laser spectrometry for multi-elemental imaging of biological tissues, Scientific reports 4 (2014) 6065.
[45] V. Piñon, M.P. Mateo, G. Nicolas, Laser-Induced Breakdown Spectroscopy for Chemical Mapping of Materials, Appl. Spectrosc. Rev. 48 (2013) 357–383.
[46] W. Dridi, J.-L. Lacour, Experimental investigation of solute transport in unsaturated cement pastes, Cement and Concrete Research 63 (2014) 46–53.
[47] S.A. Sheta, G. Di Carlo, G.M. Ingo, M.A. Harith, Surface heterogeneity study of some reference Cu-Ag alloys using laser-induced breakdown spectroscopy, Surf. Interface Anal. 47 (2015) 514–522.
[48] I. Gaona, P. Lucena, J. Moros, F.J. Fortes, S. Guirado, J. Serrano, J.J. Laserna, Evaluating the use of standoff LIBS in architectural heritage, J. Anal. At. Spectrom. 28 (2013) 810–820.
[49] D. Syvilay, A. Texier, A. Arles, B. Gratuze, N. Wilkie-Chancellier, L. Martinez, S. Serfaty, V. Detalle, Trace element quantification of lead based roof sheets of historical monuments by Laser Induced Breakdown Spectroscopy, Spectrochim. Acta Part B 103-104 (2015) 34–42.
[50] Wang M., Wang Q., Zhu M., Sun L., Peng X., Liu L., Qu J., Applying stand-off LIBS to paleoclimatic research: a case study on geochemical content of carbonate rocks, Optoelectronic Global Conference (2015).
[51] J. Rakovský, O. Musset, J. Buoncristiani, V. Bichet, F. Monna, P. Neige, P. Veis, Testing a portable laser-induced breakdown spectroscopy system on geological samples, Spectrochim. Acta Part B 74-75 (2012) 57–65.
[52] B. Connors, A. Somers, D. Day, Application of Handheld Laser-Induced Breakdown Spectroscopy (LIBS) to Geochemical Analysis, Appl. Spectrosc. 70 (2016) 810–815.
[53] C. Zhao, D. Dong, X. Du, W. Zheng, In-Field, In Situ, and In Vivo 3-Dimensional Elemental Mapping for Plant Tissue and Soil Analysis Using Laser-Induced Breakdown Spectroscopy, Sensors 16 (2016) 1–13.
[54] L. Krajcarová, K. Novotný, M. Kummerová, J. Dubová, V. Gloser, J. Kaiser, Mapping of the spatial distribution of silver nanoparticles in root tissues of Vicia faba by laser-induced breakdown spectroscopy (LIBS), Talanta 173 (2017) 28–35.
[55] V.N. Lednev, P.A. Sdvizhenskii, M.Y. Grishin, V.V. Cheverikin, A.Y. Stavertiy, R.S. Tretyakov, M.V. Taksanc, S.M. Pershin, Laser-induced breakdown spectroscopy for three-dimensional elemental mapping of composite materials synthesized by additive technologies, Appl. Opt. 56 (2017) 9698–9705.
[56] J.O. Cáceres, F. Pelascini, V. Motto-Ros, S. Moncayo, F. Trichard, G. Panczer, A. Marín-Roldán, J.A. Cruz, I. Coronado, J. Martín-Chivelet, Megapixel multi-elemental imaging by Laser-Induced Breakdown Spectroscopy, a technology with considerable potential for paleoclimate studies, Scientific reports 7 (2017) 5080–5090.

[57] M. López-López, C. Alvarez-Llamas, J. Pisonero, C. García-Ruiz, N. Bordel, An exploratory study of the potential of LIBS for visualizing gunshot residue patterns, Forensic science international 273 (2017) 124–131.
[58] S. Moncayo, L. Duponchel, N. Mousavipak, G. Panczer, F. Trichard, B. Bousquet, F. Pelascini, V. Motto-Ros, Exploration of megapixel hyperspectral LIBS images using principal component analysis, J. Anal. At. Spectrom. 33 (2018) 210–220.
[59] C. Li, X. Wu, C. Zhang, H. Ding, J. Hu, G.-N. Luo, In situ chemical imaging of lithiated tungsten using laser-induced breakdown spectroscopy, Journal of Nuclear Materials 452 (2014) 10–15.
[60] M.B. Bueno Guerra, A. Adame, E. de Almeida, Arantes de Carvalho, Gabriel Gustinelli, M.A. Stolf Brasil, D. Santos Jr, F.J. Krug, Direct analysis of plant leaves by EDXRF and LIBS: microsampling strategies and cross-validation, J. Anal. At. Spectrom. 30 (2015) 1646–1654.
[61] R.R.V. Carvalho, J.A.O. Coelho, J.M. Santos, F.W.B. Aquino, R.L. Carneiro, E.R. Pereira-Filho, Laser-induced breakdown spectroscopy (LIBS) combined with hyperspectral imaging for the evaluation of printed circuit board composition, Talanta 134 (2015) 278–283.
[62] F.J. Fortes, M.D. Perez-Carceles, A. Sibon, A. Luna, J.J. Laserna, Spatial distribution analysis of strontium in human teeth by laser-induced breakdown spectroscopy: application to diagnosis of seawater drowning, International journal of legal medicine 129 (2015) 807–813.
[63] C.M. Ahamer, K.M. Riepl, N. Huber, J.D. Pedarnig, Femtosecond laser-induced breakdown spectroscopy, Spectrochim. Acta Part B 136 (2017) 56–65.
[64] M.P. Casado-Gavalda, Y. Dixit, D. Geulen, R. Cama-Moncunill, X. Cama-Moncunill, M. Markiewicz-Keszycka, P.J. Cullen, C. Sullivan, Quantification of copper content with laser induced breakdown spectroscopy as a potential indicator of offal adulteration in beef, Talanta 169 (2017) 123–129.
[65] N. Hausmann, P. Siozos, A. Lemonis, A.C. Colonese, H.K. Robson, D. Anglos, Elemental mapping of Mg/Ca intensity ratios in marine mollusc shells using laser-induced breakdown spectroscopy, J. Anal. At. Spectrom. 32 (2017) 1467–1472.
[66] M.A. Sperança, de Aquino, Francisco Wendel Batista, M.A. Fernandes, A. Lopez-Castillo, R.L. Carneiro, E.R. Pereira-Filho, Application of Laser-Induced Breakdown Spectroscopy and Hyperspectral Images for Direct Evaluation of Chemical Elemental Profiles of Coprolites, Geostand Geoanal. Res. 41 (2017) 273–282.
[67] J.-H. Yang, S.-J. Choi, J.J. Yoh, Towards reconstruction of overlapping fingerprints using plasma spectroscopy, Spectrochim. Acta Part B 134 (2017) 25–32.
[68] K. Rifai, F. Doucet, L. Özcan, F. Vidal, LIBS core imaging at kHz speed, Spectrochim. Acta Part B 150 (2018) 43–48.
[69] T. Xu, J. Liu, Q. Shi, Y. He, G. Niu, Y. Duan, Multi-elemental surface mapping and analysis of carbonaceous shale by laser-induced breakdown spectroscopy, Spectrochim. Acta Part B 115 (2016) 31–39.
[70] R. Cerrato, A. Casal, M.P. Mateo, G. Nicolas, Dealloying evidence on corroded brass by laser-induced breakdown spectroscopy mapping and depth profiling measurements, Spectrochim. Acta Part B 130 (2017) 1–6.
[71] Y. Dixit, M.P. Casado-Gavalda, R. Cama-Moncunill, X. Cama-Moncunill, M. Markiewicz-Keszycka, P.J. Cullen, C. Sullivan, Laser induced breakdown spectroscopy for quantification of sodium and potassium in minced beef: a potential technique for detecting beef kidney adulteration, Anal. Meth. 9 (2017) 3314–3322.
[72] K. Rifai, M. Laflamme, M. Constantin, F. Vidal, M. Sabsabi, A. Blouin, P. Bouchard, K. Fytas, M. Castello, B.N. Kamwa, Analysis of gold in rock samples using laser-induced breakdown spectroscopy, Spectrochim. Acta Part B 134 (2017) 33–41.

[73] L. Sancey, S. Kotb, C. Truillet, F. Appaix, A. Marais, E. Thomas, B. van der Sanden, J.-P. Klein, B. Laurent, M. Cottier, R. Antoine, P. Dugourd, G. Panczer, F. Lux, P. Perriat, V. Motto-Ros, O. Tillement, Long-term in vivo clearance of gadolinium-based AGuIX nanoparticles and their biocompatibility after systemic injection, ACS nano 9 (2015) 2477–2488.
[74] R. Hai, C. Li, H. Wang, H. Ding, H. Zhuo, J. Wu, G.-N. Luo, Characterization of Li deposition on the first wall of EAST using laser-induced breakdown spectroscopy, Journal of Nuclear Materials 438 (2013) S1168-S1171.
[75] B. Busser, S. Moncayo, F. Trichard, V. Bonneterre, N. Pinel, F. Pelascini, P. Dugourd, J.-L. Coll, M. D'Incan, J. Charles, V. Motto-Ros, L. Sancey, Characterization of foreign materials in paraffin-embedded pathological specimens using in situ multi-elemental imaging with laser spectroscopy, Modern pathology 31 (2017) 378–384.
[76] C.D. Quarles, J.J. Gonzalez, L.J. East, J.H. Yoo, M. Morey, R.E. Russo, Fluorine analysis using Laser Induced Breakdown Spectroscopy (LIBS), J. Anal. At. Spectrom. 29 (2014) 1238–1242.
[77] S. Darwiche, M. Benmansour, N. Eliezer, D. Morvan, Laser-induced breakdown spectroscopy for photovoltaic silicon wafer analysis, Prog. Photovolt: Res. Appl. 20 (2012) 463–471.
[78] B.T. Manard, C. Derrick Quarles, E.M. Wylie, N. Xu, Laser ablation – inductively couple plasma – mass spectrometry/laser induced break down spectroscopy, J. Anal. At. Spectrom. 32 (2017) 1680–1687.
[79] M. Bonta, J.J. Gonzalez, C.D. Quarles, R.E. Russo, B. Hegedus, A. Limbeck, Elemental mapping of biological samples by the combined use of LIBS and LA-ICP-MS, J. Anal. At. Spectrom. 31 (2016) 252–258.
[80] M. Bonta, S. Török, B. Döme, A. Limbeck, Tandem LA-LIBS coupled to ICP-MS for comprehensive analysis of tumor samples, Spectrosc. Onl. 32 (2017) 42–46.
[81] X. Wang, V. Motto-Ros, G. Panczer, D. de Ligny, J. Yu, J.M. Benoit, J.L. Dussossoy, S. Peuget, Mapping of rare earth elements in nuclear waste glass–ceramic using micro laser-induced breakdown spectroscopy, Spectrochim. Acta Part B 87 (2013) 139–146.
[82] J. Li, L. Guo, N. Zhao, Q. Chen, B. Wu, Y. Wang, X. Li, J. Li, X. Zeng, Y. Lu, Analysis of ion doping profiles in Yb-doped fiber preforms using laser-induced breakdown spectroscopy, J. Anal. At. Spectrom. 31 (2016) 492–496.
[83] Hou H., Cheng L., Richardson T., Chen G. Doeff M. Zheng R., Russo R., Zorba V., Three-Dimensional Elemental Imaging of Li-ion Solid-State Electrolytes Using fs-Laser Induced Breakdown Spectroscopy (LIBS), J. Anal. At. Spectrom. 30 (2015) 2295–2302.
[84] B. Wiggins, E. Tupitsyn, P. Bhattacharya, E. Rowe, E. Lukosi, O. Chvala, A. Burger, A. Stowe, Investigation of non-uniformity and inclusions in LiInSe2 utilizing laser induced breakdown spectroscopy (LIBS), Proc. SPIE 8852 (2013) 1-11.
[85] Sweetapple M. T., Tassios S., Laser-Induced breakdown spectroscopy (LIBS) as a tool for in situ mapping and textural interpretation of lithium in pegmatite minerals, American Mineralogist 100 (2015) 2141–2151.
[86] Y. Dixit, M.P. Casado-Gavalda, R. Cama-Moncunill, X. Cama-Moncunill, M. Markiewicz-Keszycka, F. Jacoby, P.J. Cullen, C. Sullivan, Introduction to laser induced breakdown spectroscopy imaging in food, Journal of Food Engineering 216 (2018) 120–124.
[87] P. Lucena, I. Gaona, J. Moros, J.J. Laserna, Location and detection of explosive-contaminated human fingerprints on distant targets using standoff laser-induced breakdown spectroscopy, Spectrochim. Acta Part B 85 (2013) 71–77.
[88] B. Šavija, E. Schlangen, J. Pacheco, S. Millar, T. Eichler, G. Wilsch, Chloride ingress in cracked concrete, Journal of Advanced Concrete Technology 12 (2014) 425–442.

[89] P. Smyrek, Y. Zheng, H.J. Seifert, W. Pfleging, Post-mortem characterization of fs laser-generated micro-pillars in Li(Ni1/3Mn1/3Co1/3)O2 electrodes by laser-induced breakdown spectroscopy, Proc. SPIE 9736 (2016) 1-6.
[90] X. Cama-Moncunill, M. Markiewicz-Keszycka, Y. Dixit, R. Cama-Moncunill, M.P. Casado-Gavalda, P.J. Cullen, C. Sullivan, Feasibility of laser-induced breakdown spectroscopy (LIBS) as an at-line validation tool for calcium determination in infant formula, Food Control 78 (2017) 304–310.
[91] J.A. Varela, J.M. Amado, M.J. Tobar, M.P. Mateo, A. Yañez, G. Nicolas, Characterization of hard coatings produced by laser cladding using laser-induced breakdown spectroscopy technique, Appl. Surf. Sc. 336 (2015) 396–400.
[92] A. Iqbal, Z. Sun, M. Wall, Z.T. Alwahabi, Sensitive elemental detection using microwave-assisted laser-induced breakdown imaging, Spectrochim. Acta Part B 136 (2017) 16–22.
[93] P. Pořízka, S. Kaski, A. Hrdlička, P. Modlitbová, L. Sládková, H. Häkkänen, D. Prochazka, J. Novotný, P. Gadas, L. Čelko, K. Novotný, J. Kaiser, Detection of fluorine using laser-induced breakdown spectroscopy and Raman spectroscopy, J. Anal. At. Spectrom. 32 (2017) 1966–1974.
[94] I. Lopez-Quintas, M.P. Mateo, V. Piñon, A. Yañez, G. Nicolas, Mapping of mechanical specimens by laser induced breakdown spectroscopy method Application to an engine valve, Spectrochim. Acta Part B 74-75 (2012) 109–114.
[95] J.R. Chirinos, D.D. Oropeza, J.J. Gonzalez, H. Hou, M. Morey, V. Zorba, R.E. Russo, Simultaneous 3-dimensional elemental imaging with LIBS and LA-ICP-MS, J. Anal. At. Spectrom. 29 (2014) 1292–1298.
[96] L. Lin, X. Yan, X. Liao, Z. Wang, Migration and arsenic adsorption study of starch-modified Fe-Ce oxide on a silicon-based micromodel observation platform, Journal of hazardous materials 338 (2017) 202–207.
[97] O. Syta, B. Wagner, E. Bulska, D. Zielińska, G.Z. Żukowska, J. Gonzalez, R. Russo, Elemental imaging of heterogeneous inorganic archaeological samples by means of simultaneous laser induced breakdown spectroscopy and laser ablation inductively coupled plasma mass spectrometry measurements, Talanta 179 (2018) 784–791.
[98] F. Boué-Bigne, Laser-induced breakdown spectroscopy applications in the steel industry, Spectrochim. Acta Part B 63 (2008) 1122–1129.
[99] F. Boué-Bigne, Simultaneous characterization of elemental segregation and cementite networks in high carbon steel products by spatially-resolved laser-induced breakdown spectroscopy, Spectrochim. Acta Part B 96 (2014) 21–32.
[100] S. Romppanen, H. Häkkänen, S. Kaski, Singular value decomposition approach to the yttrium occurrence in mineral maps of rare earth element ores using laser-induced breakdown spectroscopy, Spectrochim. Acta Part B 134 (2017) 69–74.
[101] V. Zorba, X. Mao, R.E. Russo, Femtosecond laser induced breakdown spectroscopy of Cu at the micron/sub-micron scale, Spectrochim. Acta Part B 113 (2015) 37–42.
[102] B.D. Strycker, K. Wang, M. Springer, A.V. Sokolov, Chemical-specific imaging of shallowly buried objects using femtosecond laser pulses, Appl. Opt. 52 (2013) 4792–4796.
[103] R. Grassi, E. Grifoni, S. Gufoni, S. Legnaioli, G. Lorenzetti, N. Macro, L. Menichetti, S. Pagnotta, F. Poggialini, C. Schiavo, V. Palleschi, Three-dimensional compositional mapping using double-pulse micro-laser-induced breakdown spectroscopy technique, Spectrochim. Acta Part B 127 (2017) 1–6.
[104] S. Pagnotta, M. Lezzerini, L. Ripoll-Seguer, M. Hidalgo, E. Grifoni, S. Legnaioli, G. Lorenzetti, F. Poggialini, V. Palleschi, Micro-Laser-Induced Breakdown Spectroscopy (Micro-LIBS) Study on Ancient Roman Mortars, Appl. Spectrosc. 71 (2017) 721–727.

[105] J. Novotný, M. Brada, M. Petrilak, D. Prochazka, K. Novotný, A. Hrdlička, J. Kaiser, A versatile interaction chamber for laser-based spectroscopic applications, with the emphasis on Laser-Induced Breakdown Spectroscopy, Spectrochim. Acta Part B 101 (2014) 149–154.
[106] J. Klus, P. Mikysek, D. Prochazka, P. Pořízka, P. Prochazková, J. Novotný, T. Trojek, K. Novotný, M. Slobodník, J. Kaiser, Multivariate approach to the chemical mapping of uranium in sandstone-hosted uranium ores analyzed using double pulse Laser-Induced Breakdown Spectroscopy, Spectrochim. Acta Part B 123 (2016) 143–149.
[107] L. Krajcarová, K. Novotný, P. Babula, Provaznik I., Kucerova P., Adam V., Martin M. Z., Kizek R., J. Kaiser, Copper Transport and Accumulation in Spruce Stems (Picea abies (L.) Karsten) Revealed by Laser-Induced Breakdown Spectroscopy, International Journal of Electrochemical Science 8 (2013) 4485–4504.
[108] P. Modlitbová, K. Novotný, P. Pořízka, J. Klus, P. Lubal, H. Zlámalová-Gargošová, J. Kaiser, Comparative investigation of toxicity and bioaccumulation of Cd-based quantum dots and Cd salt in freshwater plant Lemna minor L, Ecotoxicology and environmental safety 147 (2018) 334–341.
[109] M. Abdelhamid, F.J. Fortes, M.A. Harith, J.J. Laserna, Analysis of explosive residues in human fingerprints using optical catapulting–laser-induced breakdown spectroscopy, J. Anal. At. Spectrom. 26 (2011) 1445–1450.
[110] M. Sabsabi, V. Detalle, M.A. Harith, W. Tawfik, H. Imam, Comparative study of two new commercial echelle spectrometers equipped with intensified CCD for analysis of laser-induced breakdown spectroscopy, Appl. Opt. 42 (2003) 6094–6098.
[111] C. Beresko, T. Dietz, P. Kohns, G. Ankerhold, Schnelle Materialanalyse mit Lasern, Technisches Messen 81 (2014) 537–545.
[112] C. Beresko, P. Kohns, G. Ankerhold, Surface element-mapping of three dimensional structures by laser-induced breakdown spectroscopy, Spectrochim. Acta Part B 99 (2014) 20–27.
[113] Y. Gimenez, B. Busser, F. Trichard, A. Kulesza, J.M. Laurent, V. Zaun, F. Lux, J.M. Benoit, G. Panczer, P. Dugourd, O. Tillement, F. Pelascini, L. Sancey, V. Motto-Ros, 3D Imaging of Nanoparticle Distribution in Biological Tissue by Laser-Induced Breakdown Spectroscopy, Scientific reports 6 (2016) 29936.
[114] C. Lefebvre, A. Catalá-Espí, P. Sobron, A. Koujelev, R. Léveillé, Depth-resolved chemical mapping of rock coatings using Laser-Induced Breakdown Spectroscopy, Planetary and Space Science 126 (2016) 24–33.
[115] C. Schiavo, L. Menichetti, E. Grifoni, S. Legnaioli, G. Lorenzetti, F. Poggialini, S. Pagnotta, V. Palleschi, High-resolution three-dimensional compositional imaging by double-pulse laser-induced breakdown spectroscopy, J. Inst. 11 (2016) 1-8.
[116] J. Kaiser, K. Novotný, A. Hrdlička, R. Malina, J. Novotný, D. Prochazka, M. Petrilak, L. Krajcarová, G. Vítková, P. Kučerová, Utilization of selected laser-ablation-based diagnostic methods for study of elemental distribution in various solid samples, Proc. SPIE 7746 (2010) 1–9.
[117] M. Hoehse, I. Gornushkin, S. Merk, U. Panne, Assessment of suitability of diode pumped solid state lasers for laser induced breakdown and Raman spectroscopy, J. Anal. At. Spectrom. 26 (2011) 414–424.
[118] L. Bassel, V. Motto-Ros, F. Trichard, F. Pelascini, F. Ammari, R. Chapoulie, C. Ferrier, D. Lacanette, B. Bousquet, Laser-induced breakdown spectroscopy for elemental characterization of calcitic alterations on cave walls, Environmental science and pollution research international 24 (2016) 2197–2204.

[119] J. Li, Z. Hao, N. Zhao, R. Zhou, R. Yi, S. Tang, L. Guo, X. Li, X. Zeng, Y. Lu, Spatially selective excitation in laser-induced breakdown spectroscopy combined with laser-induced fluorescence, Optics express 25 (2017) 4945–4951.
[120] C. Gottlieb, S. Millar, S. Grothe, G. Wilsch, 2D evaluation of spectral LIBS data derived from heterogeneous materials using cluster algorithm, Spectrochim. Acta Part B 134 (2017) 58–68.
[121] R. Noll, H. Bette, A. Brysch, M. Kraushaar, I. Mönch, L. Peter, V. Sturm, Laser-induced breakdown spectrometry — applications for production control and quality assurance in the steel industry, Spectrochim. Acta Part B 56 (2001) 637–649.
[122] M. Kuzuya, H. Matsumoto, H. Takechi, O. Mikami, Effect of Laser Energy and Atmosphere on the Emission Characteristics of Laser-Induced Plasmas, Appl. Spectrosc. 47 (1993) 1659–1664.
[123] F. Trichard, S. Moncayo, D. Devismes, F. Pelascini, J. Maurelli, A. Feugier, C. Sasseville, F. Surma, V. Motto-Ros, Evaluation of a compact VUV spectrometer for elemental imaging by laser-induced breakdown spectroscopy, J. Anal. At. Spectrom. 32 (2017) 1527–1534.
[124] M.A. Khater, P. van Kampen, J.T. Costello, J.-P. Mosnier, E.T. Kennedy, Time-integrated laser-induced plasma spectroscopy in the vacuum ultraviolet for the quantitative elemental characterization of steel alloys, J. Phys. D: Appl. Phys. 33 (2000) 2252–2262.
[125] S. Moncayo, F. Trichard, B. Busser, M. Sabatier-Vincent, F. Pelascini, N. Pinel, I. Templier, J. Charles, L. Sancey, V. Motto-Ros, Multi-elemental imaging of paraffin-embedded human samples by laser-induced breakdown spectroscopy, Spectrochim. Acta Part B 133 (2017) 40–44.
[126] C. Fabre, D. Devismes, S. Moncayo, F. Pelascini, F. Trichard, A. Lecomte, B. Bousquet, J. Cauzid, V. Motto-Ros, Elemental imaging by laser-induced breakdown spectroscopy for the geological characterization of minerals, J. Anal. At. Spectrom. 33 (2018) 1345–1353.
[127] R. Zeisler, Reference materials for small-sample analysis, Fresenius' J. Anal. Chem. 360 (1998) 376–379.
[128] L. Sancey, V. Motto-Ros, S. Kotb, X. Wang, F. Lux, G. Panczer, J. Yu, O. Tillement, Laser-induced breakdown spectroscopy: a new approach for nanoparticle's mapping and quantification in organ tissue, JoVE 88 (2014) 1–8.
[129] G. Alombert-Goget, F. Trichard, H. Li, C. Pezzani, M. Silvestre, N. Barthalay, V. Motto-Ros, K. Lebbou, Titanium distribution profiles obtained by luminescence and LIBS measurements on Ti, (Optical Materials) 65 (2016) 28–32.
[130] F. Trichard, F. Gaulier, J. Barbier, D. Espinat, B. Guichard, C.-P. Lienemann, L. Sorbier, P. Levitz, V. Motto-Ros, Imaging of alumina supports by laser-induced breakdown spectroscopy, Journal of Catalysis 363 (2018) 183–190.
[131] F. Trichard, L. Sorbier, S. Moncayo, Y. Blouët, C.-P. Lienemann, V. Motto-Ros, Quantitative elemental imaging of heterogeneous catalysts using laser-induced breakdown spectroscopy, Spectrochim. Acta Part B 133 (2017) 45–51.
[132] K. Kuhn, J.A. Meima, D. Rammlmair, C. Ohlendorf, Chemical mapping of mine waste drill cores with laser-induced breakdown spectroscopy (LIBS) and energy dispersive X-ray fluorescence (EDXRF) for mineral resource exploration, Journal of Geochemical Exploration 161 (2016) 72–84.
[133] S. Pagnotta, M. Lezzerini, B. Campanella, G. Gallello, E. Grifoni, S. Legnaioli, G. Lorenzetti, F. Poggialini, S. Raneri, A. Safi, V. Palleschi, Fast quantitative elemental mapping of highly inhomogeneous materials by micro-Laser-Induced Breakdown Spectroscopy, Spectrochim. Acta Part B 146 (2018) 9–15.
[134] B. Šavija, E. Schlangen, Chloride ingress in cracked concrete- a literature review, Advances in Modeling Concrete Service Life (2011) 133–142.

[135] S. Hong, W.W.-L. Lai, G. Wilsch, R. Helmerich, R. Helmerich, T. Günther, H. Wiggenhauser, Periodic mapping of reinforcement corrosion in intrusive chloride contaminated concrete with GPR, Construction and Building Materials 66 (2014) 671–684.
[136] I. Lopez-Quintas, V. Piñon, M.P. Mateo, G. Nicolas, Effect of surface topography in the generation of chemical maps by laser-induced plasma spectroscopy, Appl. Surf. Sc. 258 (2012) 9432–9436.
[137] U.A. Taparli, L. Jacobsen, A. Griesche, K. Michalik, D. Mory, T. Kannengiesser, In situ laser-induced breakdown spectroscopy measurements of chemical compositions in stainless steels during tungsten inert gas welding, Spectrochim. Acta Part B 139 (2018) 50–56.
[138] S. Imashuku, H. Taguchi, T. Kawamata, S. Fujieda, S. Kashiwakura, S. Suzuki, K. Wagatsuma, Quantitative lithium mapping of lithium-ion battery cathode using laser-induced breakdown spectroscopy, Journal of Power Sources 399 (2018) 186–191.
[139] E. Kim, H.B. Lim, Quantification of Zinc in Thermally Conducting Polycarbonate Containing Fiber-type SiO 2 Fillers, Bull. Korean Chem. Soc. 39 (2018) 341–346.
[140] P. Škarková, K. Novotný, P. Lubal, A. Jebavá, P. Pořízka, J. Klus, Z. Farka, A. Hrdlička, J. Kaiser, 2d distribution mapping of quantum dots injected onto filtration paper by laser-induced breakdown spectroscopy, Spectrochim. Acta Part B 131 (2017) 107–114.
[141] L. Sorbier, F. Trichard, S. Moncayo, C.P. Lienemann, V. Motto-Ros, Calculation of catalyst crust thickness from full elemental laser-induced breakdown spectroscopy images, IOP Conf. Ser.: Mater. Sci. Eng. 304 (2018) 1–10.
[142] J. Kaiser, K. Novotný, M.Z. Martin, A. Hrdlička, R. Malina, M. Hartl, V. Adam, R. Kizek, Trace elemental analysis by laser-induced breakdown spectroscopy—Biological applications, Surface Science Reports 67 (2012) 233–243.
[143] D. Santos, L.C. Nunes, Carvalho, Gabriel Gustinelli Arantes de, M.d.S. Gomes, P.F.d. Souza, F.d.O. Leme, Santos, Luis Gustavo Cofani dos, F.J. Krug, Laser-induced breakdown spectroscopy for analysis of plant materials: A review, Spectrochim. Acta Part B 71-72 (2012) 3–13.
[144] J. Peng, F. Liu, F. Zhou, K. Song, C. Zhang, L. Ye, Y. He, Challenging applications for multi-element analysis by laser-induced breakdown spectroscopy in agriculture: A review, TrAC 85 (2016) 260–272.
[145] M. Markiewicz-Keszycka, X. Cama-Moncunill, M.P. Casado-Gavalda, Y. Dixit, R. Cama-Moncunill, P.J. Cullen, C. Sullivan, Laser-induced breakdown spectroscopy (LIBS) for food analysis: A review, Trends in Food Science & Technology 65 (2017) 80–93.
[146] B. Busser, S. Moncayo, J.-L. Coll, L. Sancey, V. Motto-Ros, Elemental imaging using laser-induced breakdown spectroscopy, Coordination Chemistry Reviews 358 (2018) 70–79.
[147] V. Motto-Ros, L. Sancey, X.C. Wang, Q.L. Ma, F. Lux, X.S. Bai, G. Panczer, O. Tillement, J. Yu, Mapping nanoparticles injected into a biological tissue using laser-induced breakdown spectroscopy, Spectrochim. Acta Part B 87 (2013) 168–174.
[148] X. Le Guével, M. Henry, V. Motto-Ros, E. Longo, M.I. Montañez, F. Pelascini, O. de La Rochefoucauld, P. Zeitoun, J.-L. Coll, V. Josserand, L. Sancey, Elemental and optical imaging evaluation of zwitterionic gold nanoclusters in glioblastoma mouse models, Nanoscale 10 (2018) 18657–18664.
[149] A. Moussaron, S. Vibhute, A. Bianchi, S. Gündüz, S. Kotb, L. Sancey, V. Motto-Ros, S. Rizzitelli, Y. Crémillieux, F. Lux, N.K. Logothetis, O. Tillement, G. Angelovski, Ultrasmall Nanoplatforms as Calcium-Responsive Contrast Agents for Magnetic Resonance Imaging, Small 11 (2015) 4900–4909.
[150] S. Kunjachan, A. Detappe, R. Kumar, T. Ireland, L. Cameron, B. E. Douglas, V. Motto-Ros, L. Sancey, S. Sridhar, G.M. Makrigiorgos, R. Berbeco, Nanoparticle Mediated Tumor Vascular Disruption: A Novel Strategy in Radiation Therapy, ACS Nano Letter 15 (2015) 7488–7496.

[151] A. Detappe, S. Kunjachan, L. Sancey, V. Motto-Ros, D. Biancur, P. Drane, R. Guieze, G.M. Makrigiorgos, O. Tillement, R. Langer, R. Berbeco, Advanced multimodal nanoparticles delay tumor progression with clinical radiation therapy, Journal of Controlled Release 238 (2016) 103–113.